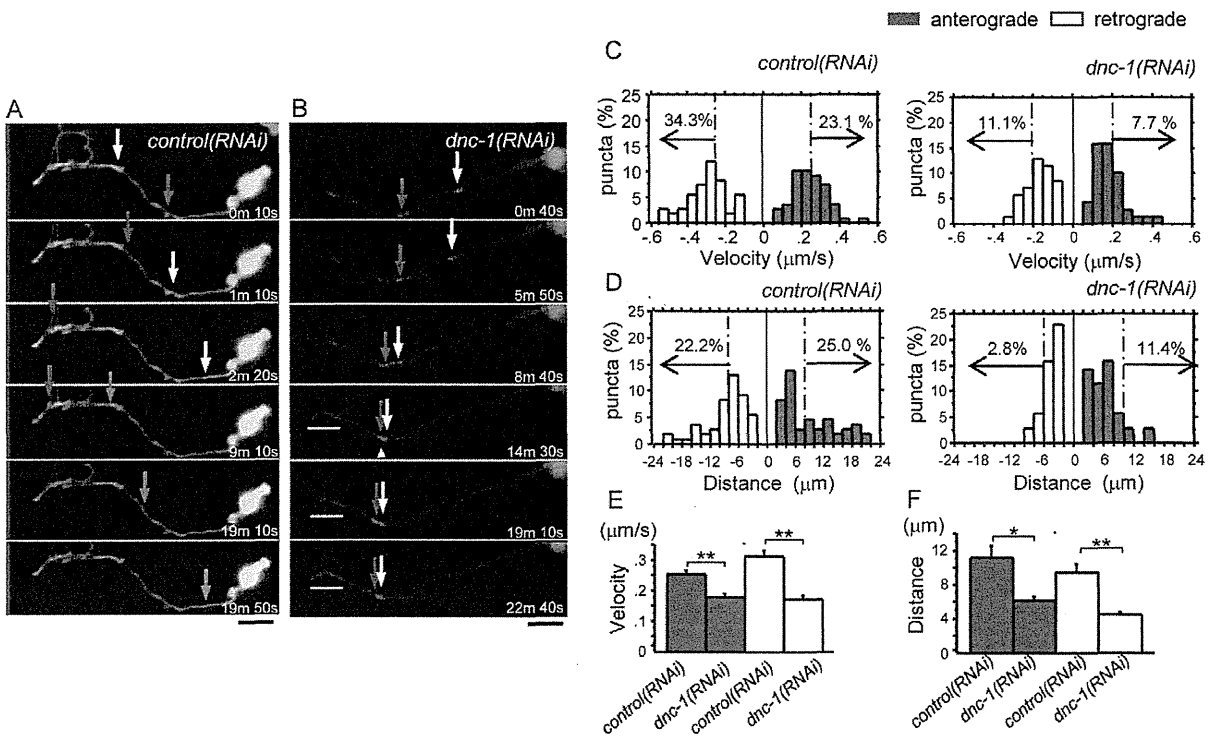

Figure 7. Impaired transport and abnormal accumulation of autophagosomes in the axons of *dnc-1(RNAi)* motor neurons. (*A, B*) Representative time-lapse images of autophagosome (DsRed-tagged Lgg1) transport in an axon (GFP-tagged shRNA; green) of a primary cultured motor neuron from the *control(RNAi)* (*A*) and *dnc-1(RNAi)* (*B*) worms. The autophagosomes were transported smoothly along the axon (arrows) of the *control(RNAi)* motor neuron (*A*). The autophagosome (arrows) was transported anterogradely, but was trapped where the axon was slightly narrowed (arrowhead) (*B*). There were also autophagosomes that accumulated in the distal part of the axon (*B*, bar). (*C*) Histograms of Lgg1::DsRed velocity in the retrograde (white bars) and anterograde (black bars) directions in neurons from the *control(RNAi)* and *dnc-1(RNAi)* worms. (*D*) Histograms of Lgg1::DsRed run-length in the *control(RNAi)* and *dnc-1(RNAi)* neurons. (*E, F*) Mean velocity (*E*) and run-length (*F*) of autophagosomes (n = 70 vesicles for each strain) in *control(RNAi)* and *dnc-1(RNAi)* neurons. Scale bar = 5 μm (A and B). The statistical analyses in *E* and *F* were performed using the Mann-Whitney U test (*$p<0.05$ and **$p<0.0001$). The error bars are S.E.M.
doi:10.1371/journal.pone.0054511.g007

Preparation of starved worms for the dietary restriction assay. All worms were synchronized by egg preparation [23]. The eggs were incubated at 20°C for 48 h in liquid medium. After 48 h, newly hatched worms were washed 3 times with distilled water, transferred to S basal medium without OP50, and incubated for 24 h. Worms were then picked randomly and used for the liquid thrashing assay.

Drug treatment. The worms were synchronized by egg preparation and incubated at 20°C for 24 h in liquid medium. They were then treated with rapamycin (LC Laboratories, Woburn, MA, USA) dissolved in ethanol at a final concentration of 10 or 100 μM, 3-methyladenine (3-MA) (SIGMA) dissolved in DMSO at a final concentration of 1 or 10 mM, or trichostatin A (TSA) (Tokyo Chemical Industry, Co., Tokyo, Japan) dissolved in DMSO at a final concentration of 1, 10, or 100 μM and incubated in liquid medium for 48 h. For controls (0 μM), ethanol or DMSO was added. Worms were then picked randomly and used for the liquid thrashing assay or microscopic analysis.

Primary neuronal cell cultures of nematodes. Primary neuronal cell cultures were prepared as described previously [24], with some modifications. In the present study, in order to obtain larger number of gravid animals, we cultured the worms in liquid medium (S basal medium with concentrated OP50) as described previously [25]. After incubation in liquid medium for 3 days, we performed egg isolation using lysis buffer (0.5 M NaOH/1% NaClO). Then we removed eggshell by enzymatic digestion using chitinase (SIGMA) and isolated embryonic cells were plated onto peanut lectin-coated glass bottom dishes (IWAKI, Tokyo, Japan).

Microscopic analysis. The worms were anesthetized by placing them in an 8-μl drop of levamisole (2 mM) on solidified pads of 2% agarose laid on slides. After coverslipping, the worms were examined under an LSM710 confocal microscope (Carl Zeiss Inc., Thornwood, NJ, USA). The regularity of SNB-1::DsRed localization/spacing was evaluated by measuring the distance between two neighboring fluorescent puncta of SNB-1::DsRed using ImageJ 1.43 software (National Institutes of Health). The axonal defasciculation index was measured as follows. The ventral nerve cord was divided into compartments consisting of two neighboring motor neurons. We counted the number of compartments with axonal defasciculation and divided it by the total number of compartments.

In vivo analysis of autophagosome mobility was performed as follows. Lgg1::DsRed worms were plated on an agar pad and observed using confocal microscopy. The red puncta, which represent autophagosomes, were observed for 1 min. The number of autophagosomes that moved within 1 min was divided by the total number of autophagosomes observed.

***In vitro* transport assay and image analysis.** Time-lapse images were acquired at room temperature using a 63× oil-immersion objective (N.A 1.4) for live-cultured neuron analysis at

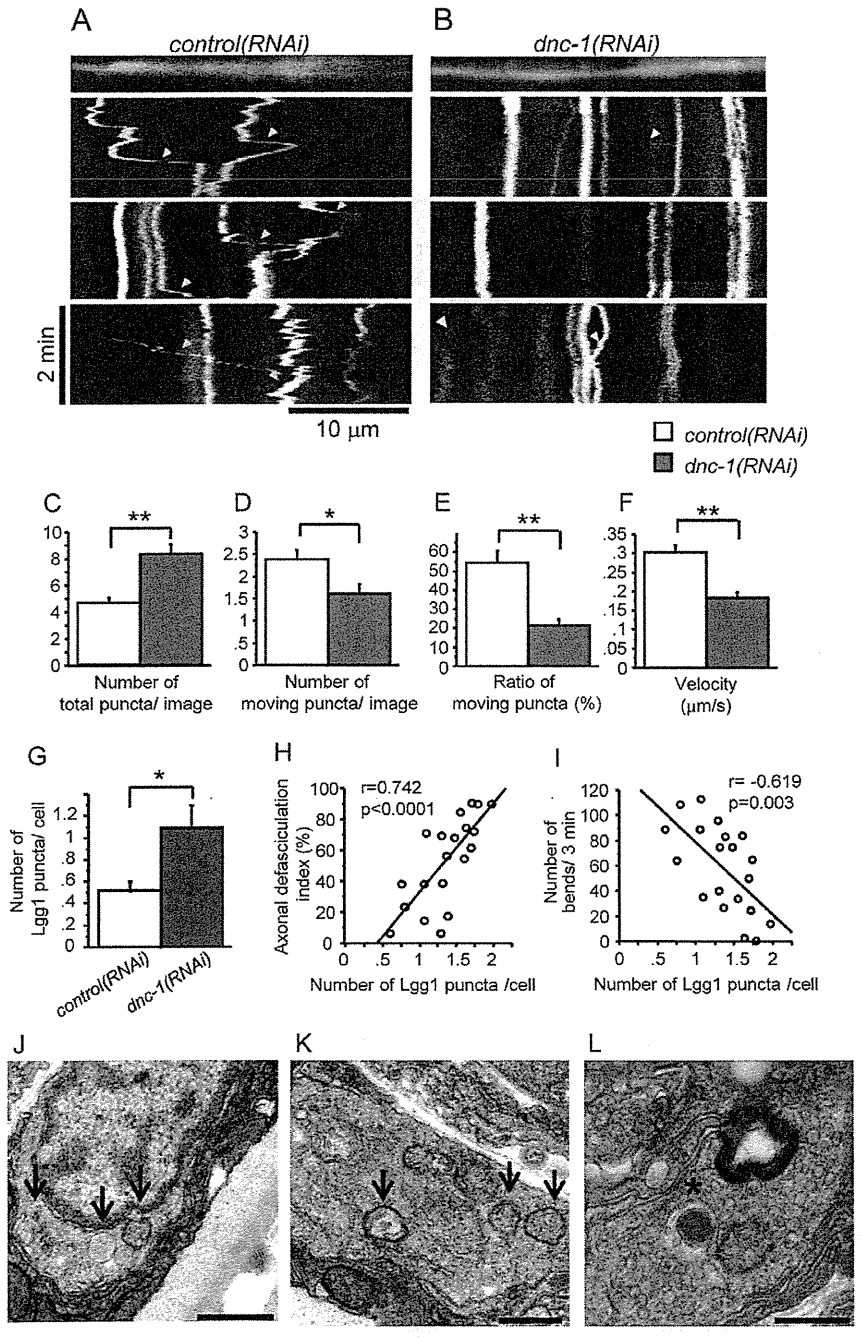

Figure 8. Accumulation of autophagosomes and motor neuron degeneration in the *dnc-1(RNAi)* worms. (*A, B*) Representative kymographs of Lgg1::DsRed in the ventral nerve cord from the *control(RNAi* (*A*) and *dnc-1(RNAi)* (*B*) worms derived from time-lapse images. Vertical lines represent stationary/docked Lgg1 puncta, while the oblique lines (labeled with arrowheads) represent the tracks of moving Lgg1 puncta. The slope of this track is an indicator of velocity. (*C*) The number of Lgg1 puncta within a single kymograph image. (*D, E*) Quantitative analyses of the mobility of puncta. The number of puncta that moved more than 2 μm was counted (*D*). The ratio of moving puncta was calculated by dividing the number of moving puncta by the total number of puncta (*E*). (*F*) The mean velocities of Lgg1 puncta. A total of 20 time-lapse images were analyzed for each strain in *C–F*. (*G*) The number of Lgg1 puncta was increased in the *dnc-1(RNAi)* worms compared with the *control(RNAi)* worms (n = 15 for each group). (*H, I*) Accumulation of autophagosomes in the *dnc-1(RNAi)* worms was correlated with the severity of axonal defasciculation (*H*) and locomotor function (*I*) (n = 20 for each analysis). (*J–L*) Ultrastructural images of ventral motor neurons from the *dnc-1(RNAi)* worms. Aberrant membranous vesicles including degenerated mitochondria were observed in the cytoplasm (*J*) and axons (*K*) (arrows). Autophagosome-like, double membrane vesicles (asterisk in *L*) were also found in the axons of the *dnc-1(RNAi)* worms (*L*). Scale bar = 500 nm (A–C) or 10 μm (D). Statistical analyses were performed using Student's t test (*$p<0.05$ and **$p<0.0001$) and Pearson's correlation coefficient in *H* and *I*. The error bars are S.E.M.
doi:10.1371/journal.pone.0054511.g008

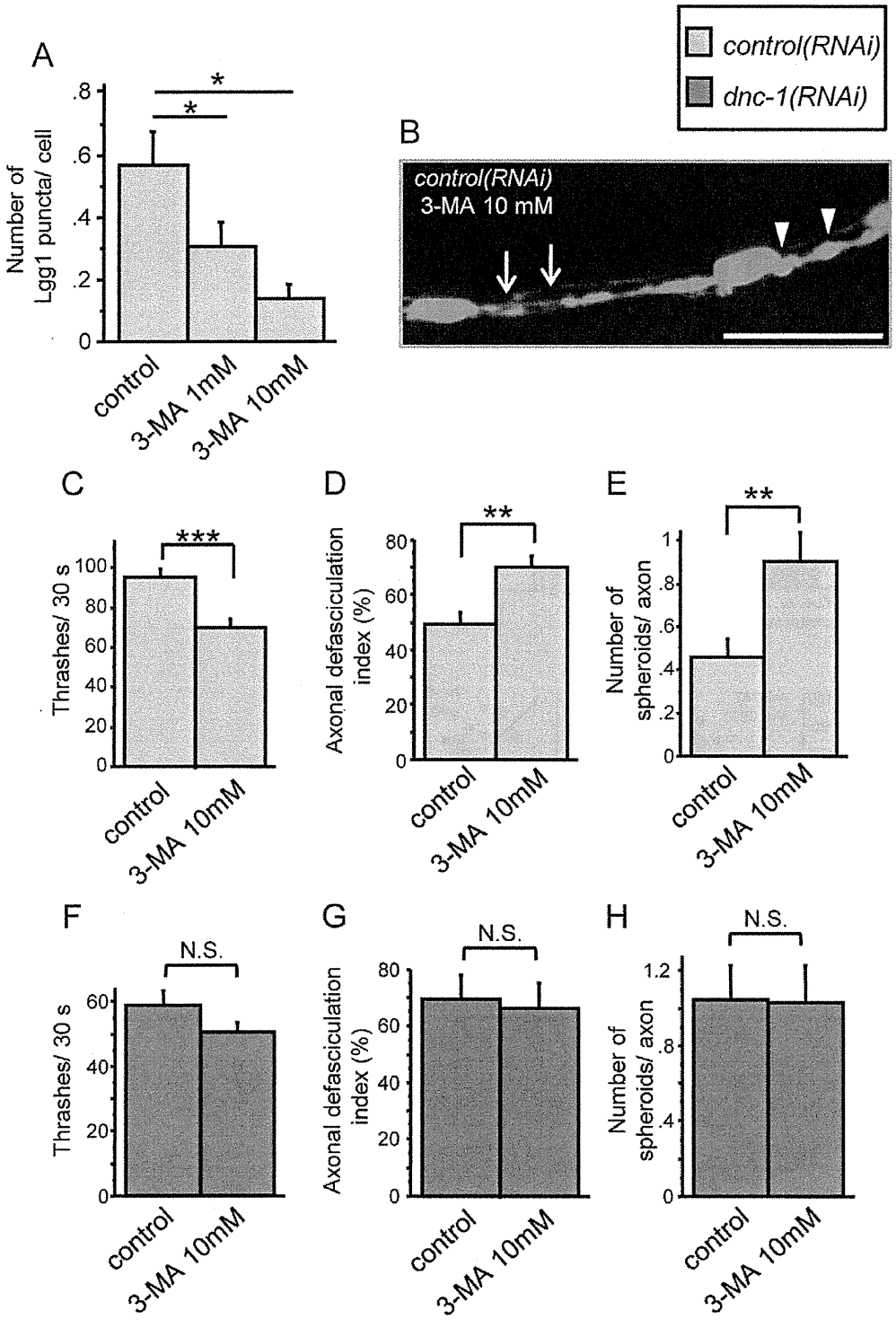

Figure 9. Dysfunction of autophagy causes axonal degeneration. (*A*) Treatment with 3-MA decreased the number of autophagosomes in the ventral nerve cord in a dose dependent manner (n = 15 for each group). (*B–E*) The effects of 3-MA on the locomotor function (*C*) and axonal morphology (*B, D,* and *E*) of the *control(RNAi)* worms. Treatment with 3-MA increased axonal defasciculation (arrows in *B* and the graph in *D*) and the number of axonal spheroids (arrowheads in *B* and the graph in *E*) (n = 15 for each group). (*F–H*) The effects of 3-MA on the locomotor function (*F*) and axonal morphology (*G, H*) of the *dnc-1(RNAi)* worms (n = 15 for each group). Scale bar = 10 μm. Statistical analyses were performed using Dunnett's post hoc test (*A*) and Student's t test (B, *D,* and *E*) (*$p<0.05$, **$p<0.001$, and ***$p<0.0001$). The error bars are S.E.M.
doi:10.1371/journal.pone.0054511.g009

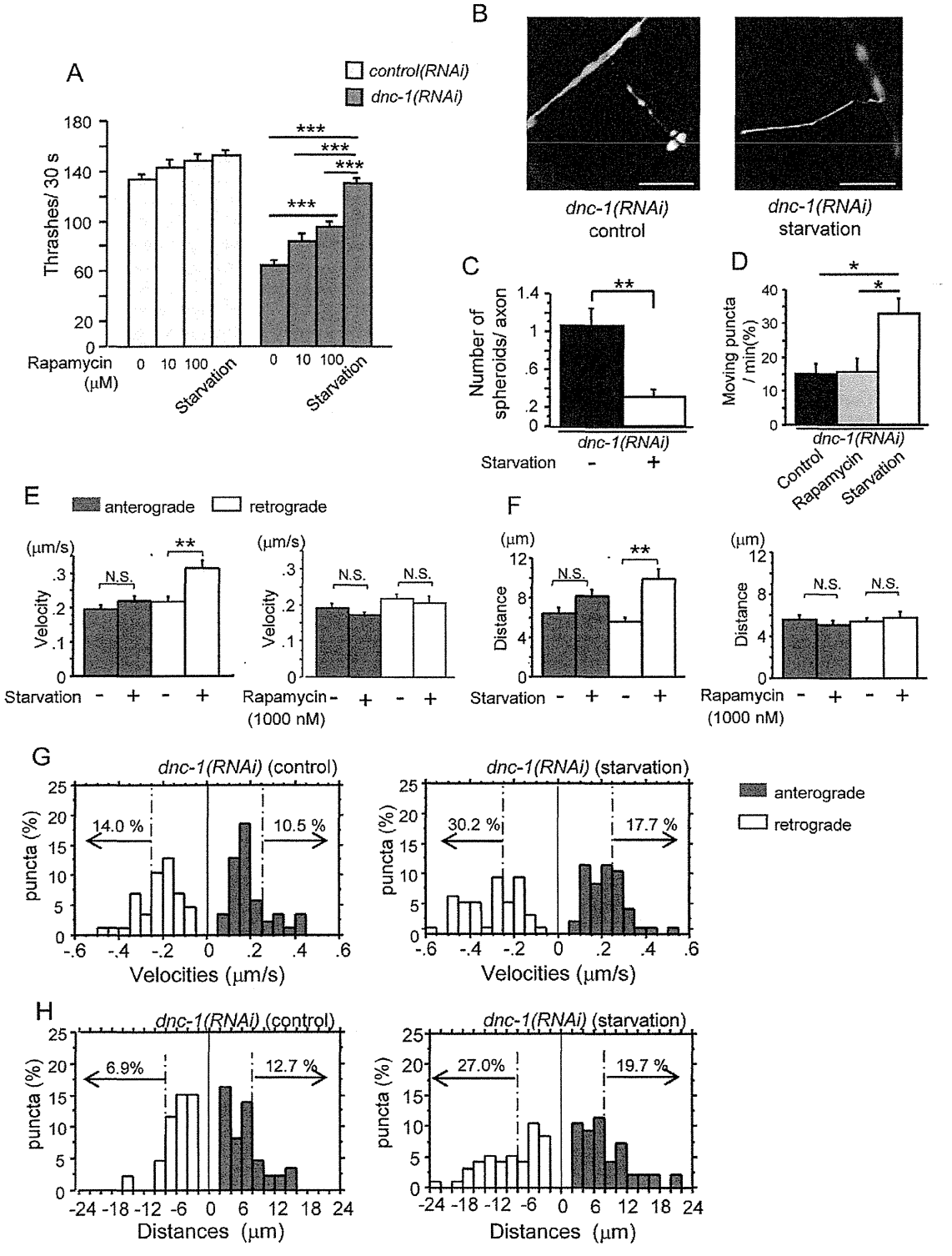

Figure 10. Starvation stimulates the retrograde transport of autophagosomes and attenuates axonal degeneration in the *dnc-1(RNAi)* worms. (*A*) Effect of rapamycin and starvation on locomotor function in the *control(RNAi)* and *dnc-1(RNAi)* worms (n = 50 for each group). (*B*) Fluorescent microscopy showing the morphological changes in axons after starvation in the *dnc-1(RNAi)* worms. (*C*) The number of axonal spheroids per transverse axon section in the *dnc-1(RNAi)* worms with or without starvation. (n = 15 animals for each treatment). (*D*) Effect of rapamycin (100 μM) and starvation on autophagosome mobility in the *dnc-1(RNAi)* worms. (n = 15 animals for each treatment). (*E, F*) Effect of rapamycin (100 μM) and starvation on the mean velocity (*E*) and run-length (*F*) of autophagosomes (black bars: anterograde transport; white bars: retrograde transport) (n = 70

vesicles for each treatment). (*G, H*) Histograms of Lgg1::DsRed velocity (*F*) and run-length (*G*) in the anterograde (black bars) and retrograde (white bars) direction in primary motor neurons from the *dnc-1(RNAi)* worms cultured with normal (control) and serum-free (starvation) medium. Scale bars = 5 μm. Statistical analyses were performed by one-way ANOVA followed by the Bonferroni/Dunn post hoc test (*A*) and Dunnett's post hoc test (*D*). Student's t test (*C*) and Mann-Whitney test (*E, F*) were used for two-group comparison (*p<0.05, **p<0.001, and ***p<0.0001). The error bars are S.E.M.

doi:10.1371/journal.pone.0054511.g010

1–2 frames/s. The images were analyzed using Zen2008 (Zeiss) software. The run-length of Lgg-1 in primary motor neurons was measured by drawing a line over moving fluorescent puncta using Zen2008. Motile puncta were counted only if they moved continuously in the same direction for more than 2 frames and if their displacement was at least 2 μm. Some runs were terminated by a pause or reversal. To ensure the accuracy of the run-length measurements, we excluded moving puncta at the beginning and end of the movie. The velocity of Lgg-1 movements was obtained from the total distance traveled divided by the duration of the run.

***In vivo* transport assay and image analysis.** Time-lapse images were acquired at room temperature using a 63× objective (N.A. 1.4) for live-worm analysis at 1 frame/s. The images were analyzed using Image J 1.43 software (National Institutes of Health). First, individual tracks of SNB-1 or Lgg1 movement were analyzed using the Multiple Kymograph plug-in, as described previously [26]. The velocity of the moving vesicles was tracked manually and their instantaneous velocity was extracted. To calculate the ratio of moving versus total vesicles, the number of vesicles that moved more than 2 μm during each time lapse period was divided with the total number of particles in each acquisition.

Electron microscopy of *C. elegans*. A conventional two-step fixation method was performed as described previously [27]. We provide the detail information in Materials and Methods S1.

Western Blot Analysis and Quantitative real-time PCR. Western blot analyses and quantitative real-time PCR were performed as described previously [28,29]. We provide a detail description in Materials and Methods S1.

Statistical analysis. Statistical analyses were performed using StatView software version 5 (Hulinks, Tokyo, Japan). We used the Kaplan-Meier and log-rank test, Student's t-test, Mann-Whitney U test, and one-way analysis of the variance (ANOVA) with the Bonferroni or Dunnett's post-hoc test. Pearson's correlation coefficient was used to assess the correlation of variables.

Results

Dysregulated dynactin 1 expression and autophagy in degenerated spinal motor neurons in SALS patients

The expression of the *DCTN1* gene was markedly reduced in the spinal motor neurons of SALS patients, as reported previously [9,13] (Fig. 1*A*). Recent studies indicate that the dysregulation of autophagy in motor neurons is a pivotal event in ALS [8,10]; thus, we investigated the relationship between decreased dynactin 1 expression and autophagy in SALS. Immunohistochemistry using consecutive sections of autopsied human spinal cords revealed that LC3 immunoreactivity, a histological marker of autophagy, was increased in the motor neurons of SALS patients in which dynactin 1 expression was decreased (Fig. 1*B*). Conversely, there was no change in the immunoreactivity for dynactin 1 and LC3 in cerebellar Purkinje cells, which showed no degeneration (Fig. 1*C*). Quantitative analysis revealed that anti-LC3 immunoreactivity was significantly increased in the spinal motor neurons of SALS patients ($p<0.0001$) (Fig. 1*D*), and was inversely correlated with the decreased mRNA levels of *DCTN1* (Fig. 1*E*) and cell size (Fig. 1*F*) in the motor neurons of SALS patients, indicating that the dysregulation of autophagy is associated with the decreased expression of dynactin 1 in SALS. Electron microscopy of sections from the SALS and control patients (Fig. 1*G, H*) also revealed that there was an abundance of autophagic vacuoles, e.g., multilamellar bodies (arrowheads in Fig. 1*I, K*), autophagosome-like double membrane vesicles (arrows in Fig. 1*K, J*), and autolysosomes (asterisks in Fig. 1*L*) in the motor neurons of the SALS patients, which were scarcely observed in the control patients.

Generation of the *dnc-1*-depleted *C. elegans* model

To examine the relationship between the loss of dynactin 1, the accumulation of autophagosomes, and motor neuron degeneration, we created a *dnc-1*-KD *C. elegans* model by transfecting *C. elegans* with a plasmid expressing an shRNA and GFP under the control of the motor neuron-specific *acr2* promoter (*dnc-1(RNAi)*). In the transgenic worms, GFP was expressed diffusely in ventral motor neurons (Fig. 2*A*). We confirmed the effect of RNA interference on the level of endogenous *dnc-1* mRNA using whole mount *in situ* hybridization. In the *control(RNAi)* worms, *dnc-1* expression was not altered by *shRNA::GFP* expression (Fig. 2*B*). Conversely, in the *dnc-1(RNAi)* worms, motor neurons expressing *shRNA::GFP* exhibited reduced or no expression of *dnc-1* (Fig. 2*B*). As shown in Fig. 2*C*, approximately 22 neurons were GFP-positive both in the *control(RNAi)* and *dnc-1(RNAi)* worms. The number of *dnc-1*-positive motor neurons was decreased by approximately 20 (*control(RNAi)* worms, 35.3±3.8; *dnc-1(RNAi)* worms, 15.9±9.8), suggesting that *dnc-1* was successfully knocked down in almost all the GFP-positive cells (Fig. 2*C, D*). Moreover, *dnc-1* expression was not affected in the head sensory neurons of the *dnc-1(RNAi)* worms, confirming the specificity of the promoter (Fig. 2*E*). Taking these results into account, in the following experiments, we selected the *dnc-1(RNAi)* and *control(RNAi)* worms expressing GFP in more than 30 motor neurons to avoid the influence of knockdown efficiency on the experimental results.

Motor dysfunction in motor neuron-specific *dnc-1*-KD *C. elegans*

The *dnc-1(RNAi)* worms demonstrated uncoordinated locomotion (Fig. 3*A*), which is a phenotype observed in *C. elegans* mutant models of motor neuronal defects [30,31]. Maturation of the worms resulted in the progressive aggravation of their uncoordinated locomotion, characterized by partial paralysis, slowed movement, and coiling. The feeding plate of the *dnc-1(RNAi)* worms appeared to be stagnated, as they only ate the food around themselves due to their decreased motility (Fig. 3*A*). As described in the Materials and Methods, we generated six lines of *dnc-1(RNAi)* worms: SBG7, 8, and 15 using shRNA1(101), and SBG20, 24, and 25 using shRNA2(2888). Survival analysis and body bend assays were performed using these six lines. Since these animals exhibited almost the same phenotype, SBG8 was employed for further analysis. Compared with the *control(RNAi)* worms, the *dnc-1(RNAi)* worms had a decreased life span (Fig. 3*B, C*) (11.4±4.4, 11.2±3.0, 13.4±4.0, and 14.3±3.3 days for *dnc-1(RNAi-1)*, *dnc-1(RNAi-2)*, *control(RNAi)*, and wild-type worms, respectively). *dnc-1(RNAi)* worms also exhibited significantly reduced bending and thrashing rates that declined with age

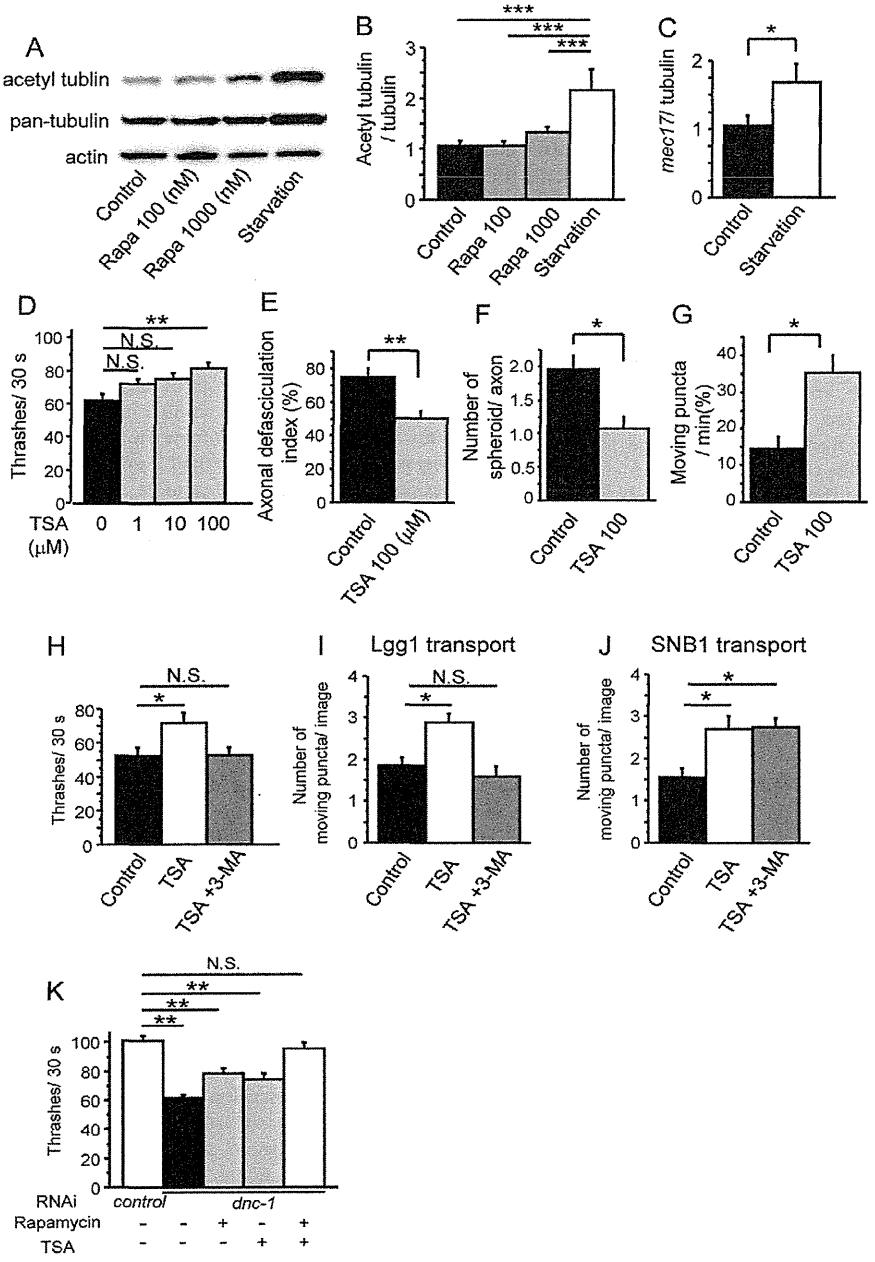

Figure 11. The effects of tubulin acetylation on the transport of autophagosome and neurodegeneration in the *dnc-1(RNAi)* worms. (*A, B*) Immunoblots of primary cultured cells using antibodies against acetylated tubulin, pan-tubulin, and actin (n = 5). (*C*) The mRNA levels of *mec17* measured by real-time RT-PCR. The data shown are ratios to the mRNA levels of *tba1*, the gene encoding alpha-tubulin. (*D*) Effect of trichostatin A (TSA) on the locomotor function of the *dnc-1(RNAi)* worms (n = 35 for each group). (*E–G*) Effect of TSA (100 μM) on the axonal degeneration of the *dnc-1(RNAi)* worms (*E, F*) and on autophagosome mobility (*G*) (n = 15 for each group). (*H*) The inhibition of autophagy by 3-MA (10 mM) negates the effect of TSA treatment on the motor function of the *dnc-1(RNAi)* worms (n = 35 for each group). (*I, J*) The number of moving puncta (*I*, Lgg1; *J*, SNB1) was counted using kymographs derived from *in vivo* time-lapse images (n = 20 images for each analysis). Treatment with 3-MA negates the effect of TSA treatment on the transport of Lgg1 (*I*), but not the transport of SNB1 (*J*). (*K*) Combination therapy of rapamycin (100 μM) and TSA (100 μM) has synergistic effects on the locomotive functions of the *dnc-1(RNAi)* worms (n = 35 for each group). Statistical analyses were performed by one-way ANOVA followed by the Bonferroni/Dunn post hoc test for (*B*), Dunnett's post hoc test (*D, H–K*), and Student's t test (*C, E–G*) (*p<0.05, **p<0.001, and ***p<0.0001). The error bars are S.E.M.
doi:10.1371/journal.pone.0054511.g011

(Fig. 3*D, E*). The thrashing speed of the *control(RNAi)* worms was slightly decreased compared with the wild-type worms, possibly due to the toxicity of GFP, as previously reported [32] (Fig. 3*E*). Although the toxicity of GFP was much less than that of *dnc-1* knockdown and not detectable in the bending assay, to exclude any effects of the fluorescent protein on our analysis, we compared

the *dnc-1(RNAi)* worms with the *control(RNAi)* worms, both of which express GFP at similar levels, in all experiments. We also performed a video capture analysis to visualize the movement trace of each worm and measure its average speed (Fig. 3*F, G*). The movement speed was dramatically decreased in the *dnc-1(RNAi)* worms compared with the *control(RNAi)* worms at an early adult stage.

Axonal degeneration is the early sign of neurodegeneration in the *dnc-1(RNAi)* worms

We then examined the morphological changes in the *dnc-1(RNAi)* worms using fluorescent microscopy. In normal worms, the ventral nerve cords were tightly fasciculated and the motor-neuron cell bodies (white asterisks in Fig. 4*A*) were round or ovoid. (Fig. 4*B, C*). By contrast, we found irregular shapes and defasciculation of the ventral nerve cord as well as axonal swellings, or spheroids, in the *dnc-1(RNAi)* worms at an early stage (Fig. 4*D*). At this early stage (4 days old), the cell bodies in the *dnc-1(RNAi)* worms seemed normal judging from their shape and structure (Fig. 4*D*). However, at a later adult stage (7 days old), axonal degeneration was exacerbated and morphological changes were also detected in the cell bodies (Fig. 4*E*). Axonal changes were occasionally observed in the *control(RNAi)* worms with aging, but they were less frequent and not as severe as in the *dnc-1(RNAi)* worms (Fig. 4*C*). Semi-quantification of the axonal and cell body changes showed that the axonal abnormalities were observed at day 4 and cell body deformation occurred at a later stage (Fig. 4*F*). Although some neurons exhibited an abnormal cell body shape at day 4, this change was only observed in the worms with axonal defasciculation (Fig. 4*G*), indicating that axonal degeneration occurs prior to cell body degeneration. Moreover, we also found that the severity of axonal defasciculation (i.e., the axonal defasciculation index) was correlated with locomotor dysfunction in the *dnc-1(RNAi)* worms (Fig. 4*H*). To clarify the time-course of the neuronal changes due to *dnc-1* depletion, we also examined the morphological change during the developmental stage. The acr2p::shRNA::GFP is not detectable before larval stage L1 (Fig. S1*A–C*). Furthermore, even after GFP is expressed, there was no alteration in morphology or motor phenotype during the larval stage (from L1 to L4, post natal days 1 and 2) (Fig. S1*C–E*). It was only after the worms became adult that the axonal degeneration and motor deficit appeared. Taken together, these findings suggest that the depletion of *dnc-1* induces the degeneration, rather than developmental defects, of motor neurons in *C. elegans*.

Further analysis via electron microscopy confirmed the axonal degeneration in the *dnc-1(RNAi)* worms (Fig. 5*C–F*). In the early degenerative stage, *dnc-1(RNAi)* worms first exhibited whorl like inclusions in axons with only a few morphological changes in their cell bodies (Fig. 5*C, D*) compared with *control(RNAi)* worms (Fig. 5*A, B*). In the later degenerative stage, strikingly abundant whorl-like inclusions and vacuoles, corresponding to degeneration and swelling of axons [21], were observed in axons and cell bodies (Fig. 5*E, F*).

Axonal transport defect in the *dnc-1(RNAi)* worms

Abnormalities in the localization and accumulation of synaptic vesicles were reported in a *C. elegans* model showing a defect in axonal transport [20]. To determine whether our *dnc-1(RNAi)* model exhibited defects in axonal transport, we used a fluorescently tagged synaptic vesicle marker composed of the *C. elegans* VAMP2/synaptobrevin protein fused to DsRed (SNB-1::DsRed), and examined the distribution of the dorsally located red puncta (Fig. 6*A*). In the dorsal nerve cord (the axons of the ventral motor neurons) of the *control(RNAi)* worms, SNB-1::DsRed puncta were regularly spaced, whereas the *dnc-1(RNAi)* worms exhibited a discontinuous and irregular distribution of the marker, including occasional clumps that may represent the accumulation of cargo proteins (Fig. 6*B*). Histograms of the distances between neighboring SNB-1 puncta displayed a broader curve in the *dnc-1(RNAi)* worms than in the *control(RNAi)* worms, suggesting some defect in axonal transport caused by the knockdown of *dnc-1* (Fig. 6*C, D*).

To demonstrate direct evidence of a defect in axonal transport in our transgenic worms, we monitored the movement of SNB-1 puncta by acquiring a series of time-lapse images. The resulting kymographs showed that puncta in the *dnc-1* KD worms were markedly static compared with those in the controls, confirming the disruption of axonal transport following the reduction of *dnc-1* in *C. elegans* (Fig. 6*E, F*, Movies S1, S2). To quantify the movement of SNB-1, we analyzed 20 kymographs from each strain. While there was no significant difference in the number of SNB-1 puncta between the *control(RNAi)* and *dnc-1(RNAi)* worms (Fig. 6*G*), the number of moving puncta (moving more than 2 μm) (Fig. 6*H*) and the ratio of moving puncta to total puncta (Fig. 6*I*) were significantly decreased in the *dnc-1(RNAi)* worms compared to the *control(RNAi)* worms ($p = 0.028$ and $p = 0.014$, respectively). The velocity of SNB-1 transport in the *dnc-1(RNAi)* worms was significantly lower than in the *control(RNAi)* worms ($p < 0.0001$, Fig. 6*J*).

Impaired transport and accumulation of autophagosomes in the *dnc-1(RNAi)* worms

We next investigated the effects of *dnc-1* depletion on autophagy in *C. elegans*. Autophagosomes are cargo that moves bidirectionally along microtubules, powered by the kinesin family of motor proteins and dynein/dynactin complexes [11,12]. Altered autophagy has been observed in several neurodegenerative models, including the mutant *DCTN1* mouse model [9,16,33,34]. However, little is known about the relationship between the decreased levels of dynactin 1 and the alteration of autophagy. To clarify the effect of quantitative loss of DNC-1/dynactin 1 in the transport of autophagosomes, we performed live-cell imaging analyses of autophagosome transport in the axons of primary cultured motor neurons from the *dnc-1(RNAi)* and *control(RNAi)* worms that co-expressed DsRed-tagged Lgg1/ATG8, which is associated with the autophagic membrane, in ventral motor neurons under the control of the *acr2* promoter (Mizushima et al. [35]. This marker of autophagosomes is expressed diffusely in the ventral motor neurons (Fig. S2*A*) and forms distinct puncta when autophagosomes are formed (Fig. S2*B*) [36]. In the *control(RNAi)* neurons, the fluorescent Lgg1 vesicles moved toward and away from the cell body, suggesting that these vesicles are powered by anterograde and retrograde motors (Fig. 7*A*, Movie S3). By contrast, in the *dnc-1(RNAi)* worms, the autophagosomes were easily trapped where the axon was tight or curved, or at spheroids (Fig. 7*B*, Movie S4). This phenomenon was followed by the accumulation of autophagosomes distal to the trapped sites. Histograms showing the distribution of the velocity and distance of autophagosome movement demonstrated a significant loss of fast- and long-moving vesicles in the *dnc-1(RNAi)* cells compared with the *control(RNAi)* cells (Fig. 7*C, D*). The mean velocity and movement distance (run-length) were significantly decreased in the anterograde and retrograde directions in the *dnc-1(RNAi)* neurons ($p < 0.0001$, $= 0.0001$; velocity of anterograde, retrograde movements, respectively, and $p = 0.0045$, < 0.0001; run-length of anterograde, retrograde movements, respectively) (Fig. 7*E, F*).

Next, we performed kymograph analysis of Lgg1::DsRed using *in vivo* time-lapse images (Fig. 8*A, B*, Movie S5, S6). Although the total number of Lgg1 puncta was significantly increased

($p<0.0001$) (Fig. 8*C*), the number (Fig. 8*D*) and the ratio of moving puncta (Fig. 8*E*) were significantly decreased in the *dnc-1(RNAi)* worms compared with the *control(RNAi)* worms ($p = 0.013$ and $p<0.0001$, respectively). The velocity of Lgg1 movement was also significantly decreased in the *dnc-1(RNAi)* worms ($p<0.0001$) (Fig. 8*F*). These results indicated that the *dnc-1* depletion resulted in the accumulation of untransported autophagosomes in the motor neurons.

We then investigated whether the accumulation of autophagosomes is related to the motor neuron degeneration. In the ventral nerve cord of the *dnc-1(RNAi)* worms, the number of Lgg1 puncta was significantly increased in comparison with the *control(RNAi)* worms ($p = 0.019$) (Fig. 8*G*), and the accumulation of autophagosomes was correlated with the axonal defasciculation index and locomotor function (Fig. 8*H, I*). We also explored the localization of Lgg1::DsRed in the distal ascending axon and observed Lgg1::DsRed accumulation in axonal spheroids (Fig. S2*C*), which is consistent with a previous report showing the abnormal accumulation of disorganized organelles and autophagosomes in axonal spheroids [37]. Electron microscopy showed that the accumulation of vesicular structures, including autophagosome-like vesicles and mitochondria, was observed in the proximal axons or cytoplasm of the *dnc-1(RNAi)* worms, although such accumulations were detected rarely in the axons of the *control(RNAi)* neurons (Fig. 8*J–L*).

We then treated the *control(RNAi)* worms with 3-MA, which inhibits the formation of autophagosomes (Fig. 9*A*). These worms showed the locomotory defects and axonal degeneration observed in the *dnc-1(RNAi)* worms, suggesting that the disrupted autophagy system is sufficient to cause the motor neuronal degeneration in this model (Fig. 9*B–E*). On the other hand, when we treated the *dnc-1(RNAi)* worms with 3-MA, worms did not exhibit a substantial change in the motor function or in the axonal integrity (Fig. 9*F–H*).

Starvation dramatically attenuates the motor deficits in the *dnc-1(RNAi)* worms by facilitating the axonal transport of autophagosomes

Autophagy is known to be activated by rapamycin, a specific inhibitor of the mTOR pathway [38]. Starvation is also a strong activator of autophagy; however, it also has other effects, e.g., activation of the mitogen-activated protein kinase (MAPK) pathway [39], stimulation of tubulin acetylation [40], and induction of sirtuin [41]. Both treatments have been used widely in many species, e.g., *Drosophila*, mouse, and *C. elegans*, to activate autophagy [42–44].

To study the effects of autophagy activators on axonal degeneration in *C. elegans*, we treated the *control(RNAi)* and *dnc-1(RNAi)* worms with rapamycin or starved them by food restriction, and investigated the changes in motor function via the liquid thrashing assay. Rapamycin and starvation are known to extend lifespan of *C. elegans* [42,45]. In the present study, we found that neither rapamycin nor starvation significantly altered the motor function of the *control(RNAi)* worms (Fig. 10*A*). In the *dnc-1(RNAi)* worms, rapamycin ameliorated the thrashing activity in a dose-dependent manner, although it showed only a limited effect even at the most effective dose (Fig. 10*A*). In contrast, starvation completely ameliorated the motor dysfunction of the *dnc-1(RNAi)* worms without affecting the efficiency of *dnc-1* knockdown (Fig. 10*A*, Fig. S3*A–C*). The formation of axonal spheroids was also significantly suppressed by starvation ($p = 0.001$) (Fig. 10*B, C*). Given the differential effects of rapamycin and starvation, we hypothesized that starvation not only increases the formation of autophagosomes but also increases their mobility in axons. Indeed, the frequency of autophagosome movement was increased by food restriction (Fig. 10*D*). To further confirm this hypothesis, we cultured primary motor neurons from the *dnc-1(RNAi)* worms in serum-depleted medium, and quantified the mobility of autophagosomes by monitoring the movement of DsRed-tagged Lgg1 in axons. As we expected, starvation significantly increased the speed and run-length of moving Lgg1 puncta, especially the retrograde run-length, in the *dnc-1(RNAi)* worms ($p<0.0001$) (Fig. 10*E, F*). Conversely, neurons treated with rapamycin showed no detectable change in the transport of autophagosomes (Fig. 10*E, F*). Histograms showing the distribution of the velocity and distance of autophagosome movement also demonstrated a significant increase of fast- and long-moving vesicles in the starved cells, especially in retrograde transport (Fig. 10*G, H*). For example, the percentage of vesicles that moved more than 8 μm retrogradely increased from 6.9% (*dnc-1(RNAi)* control) to 27.0% (*dnc-1(RNAi)* starvation), whereas the change was only from 12.7% to 19.7% in the anterograde direction (Fig. 10*H*).

Finally, we investigated how starvation stimulates the axonal transport of autophagosomes and assessed whether drugs that mimic the molecular mechanisms of starvation enhanced its effect. The acetylation of tubulin is known to stabilize microtubules and activate axonal transport by the subsequent recruitment of the molecular motors kinesin-1 and dynein/dynactin to microtubules [46,47]. Therefore, we assessed the acetylation state of alpha-tubulin in our cultured cell assay. Starvation increased the levels of acetylated tubulin, but this effect was not detected in cells treated with rapamycin (Fig. 11*A, B*). Moreover, real-time quantitative PCR demonstrated that starvation, but not rapamycin, significantly increased the mRNA levels of *mec-17*, an enzyme that acetylates tubulin in *C. elegans* [48] (Fig. 11*C*). Taken together, our results suggest the possibility that starvation mitigated axonal degeneration by activating autophagy and promoting the axonal transport of autophagosomes via the acetylation of tubulin in the *dnc-1(RNAi)* worms. To test this hypothesis, we examined the effects of TSA, an HDAC inhibitor that facilitates tubulin acetylation, on the phenotypes of the *dnc-1(RNAi)* worms. Although treatment with TSA did not exhibit substantial effects on the phenotype of the *control(RNAi)* worms (Fig. S4*A–C*), this treatment showed a significant effect on the locomotory function of the *dnc-1(RNAi)* worms in a dose-dependent manner, and attenuated the axonal degeneration without alteration of *dnc-1* knockdown efficiency (Fig. 11*D–F*, Fig. S3*A, B, and D*). As expected, TSA increased the mobility of autophagosomes (Fig. 11*G*). Interestingly, treatment with 3-MA dampened the effect of TSA on locomotion (Fig. 11*H*). On the contrary, the worms treated with both TSA and 3-MA showed decreased transport of autophagosomes without defects in the transport of synaptobrevin (Fig. 11*I, J*). Furthermore, we also examined the effect of combination therapy with rapamycin and TSA. Although treatment with rapamycin or TSA alone had limited effects in comparison with *control(RNAi)* worms, the combination of rapamycin and TSA had greater effects such that locomotion was restored in the worms treated with these two drugs to the levels observed in the *control(RNAi)* worms (Fig. 11*K*).

Discussion

In the present study, we generated a novel *C. elegans* model that mimics the down-regulation of dynactin 1 observed in the motor neurons of SALS patients. Using this model, we investigated whether the quantitative loss of DNC-1/dynactin 1 causes motor neuron degeneration. Our results showed that the knockdown of *dnc-1* caused progressive motor deficits in *C. elegans*, and the

pathological changes observed in this model shared several features with those seen in SALS patients, e.g., the axonal accumulation of membranous structures, such as mitochondria and autophagosomes, and motor neuron degeneration characterized by axonal degeneration including axonal spheroids. We also observed the disrupted transport of autophagosomes in the degenerated motor neurons of this model. Interestingly, our model exhibited adult-onset motor neuron degeneration even though the *shRNA::gfp* had already expressed in the larval stage. Given that the patients carrying mutant *DCTN1* and SALS patients exhibit an adult-onset motor neuron degeneration, it is possible that developing motor neurons are resistant to the disruption of DNC-1/dynactin 1. However, differentiated motor neurons may be vulnerable to the detrimental effects of dynactin 1 depletion, since they require more efficient transport system to maintain axonal homeostasis than developing neurons. Together, these findings indicate that this *dnc-1*-KD *C. elegans* model is a powerful tool for understanding the relationship between the disrupted transport of autophagosomes, neurodegeneration, and motor phenotype.

The mechanism of autophagosome accumulation in motor neurons harboring a motor protein abnormality was shown directly by our analysis of autophagosomal transport; namely, the knockdown of *dnc-1* decreased the transport of autophagosomes and shortened their run-length. Physiological cargoes typically use multiple motors, and their run-lengths are correlated with the number of coordinated motor proteins [49]. Our results showed that the knockdown of *dnc-1* reduced the speed and distance of retrograde transport by approximately half. These results are consistent with previous *in vitro* studies of dynein showing that the run-length of retrograde motor complexes is reduced by approximately half in cells lacking dynactin 1 [49,50]. Our data indicated that the knockdown of *dnc-1* also affected the anterograde transport of autophagosomes, which is consistent with previous reports showing that a defect in retrograde transport led to dysregulated movements in both directions [51,52].

The relationship between the decreased DNC-1/dynactin 1 levels, the increased number of autophagosomes, and axonal degeneration was confirmed by our observations that the *dnc-1(RNAi)* worms showed an abnormal accumulation of autophagosomes and that their locomotory defects and axonal degeneration were correlated with the accumulation of autophagosomes. Furthermore, the *control(RNAi)* worms treated with 3-MA, an inhibitor of autophagy, showed the same phenotype as the *dnc-1(RNAi)* worms, including defective locomotory function and degenerated axons. Taken together, our findings in the *dnc-1(RNAi) C. elegans* model provide direct evidence that the lack of DNC-1/dynactin 1 in dynein/dynactin motor complexes leads to slow, short-distance movements of autophagosomes, followed by their axonal accumulation, and neurodegeneration.

It is clinically important to determine whether the activation of autophagy could be an effective therapeutic strategy against neurodegenerative diseases, especially when the transport of autophagosomes is disrupted. In previous studies, the effects of rapamycin, which induces autophagosome formation [9], against models of neurodegeneration were controversial [53–55]. In the present study, rapamycin only slightly ameliorated the motor dysfunction of the *dnc-1(RNAi)* worms, although its effects were substantially enhanced by the addition of TSA which enhances the acetylation of tubulin. Given that tubulin acetylation was shown to stimulate axonal transport [47], our results suggest that combination therapy with rapamycin and TSA, attenuated the neurodegeneration and locomotory dysfunction of this model by facilitating the formation and axonal transport of autophagosomes.

Although it is still possible that the disrupted transport of other organelles such as mitochondria are also involved in the pathogenesis of motor neuron degeneration in the *dnc-1(RNAi)* worms, the observation that 3-MA, an inhibitor of autophagy, almost completely abrogated the benefit effects of TSA suggests a substantial role for autophagosomal transport in the functional maintenance of motor neurons. This view is further supported by the fact that the worms treated by both TSA and 3-MA showed the decreased transport of autophagosomes without defects in the transport of synaptobrevin.

In conclusion, we found that decreased levels of dynactin 1 in motor neurons induce neurodegeneration at least partially via the disruption of the axonal transport of autophagosomes. The therapeutic strategy we examined in this study could be expanded to other neurodegenerative disorders, since the accumulation of autophagosomes and disrupted axonal transport are common features of many neurodegenerative diseases. Future study is needed to explore the effectiveness and safety of the treatments that stimulate the transport of autophagosomes in the mammalian central nervous system.

Supporting Information

Figure S1 Expression pattern of *shRNA*::GFP and morphology of ventral motor neurons during embryonic and larval stage. (*A, B*) Representative confocal micro scopic image of *shRNA*::GFP expression during embryonic stages. GFP was not observed in the eggs even after delivery (asterisks in *A, B*). (*C–E*) GFP expression were observed in the ventral motor neurons (black arrows in *C*) from L1 (larval 1) stage of the worms. The ventral nerve axons (white arrows in *D, E*) did not exhibit abnormal changes such as axonal swellings or defasciculations during L1-4. Scale bars = 20 μm (*A–C*), 100 μm (low magnification image in *D, E*), or 50 μm (high magnification in *D, E*).
(TIF)

Figure S2 Expression pattern of the Lgg1::DsRed in the *control(RNAi)* worm and the *dnc-1(RNAi)* worm. (*A, B*) Representative fluorescent microscopic views of the Lgg1::DsRed in the ventral nerve cord of *control(RNAi)* worms (*A*) and *dnc-1(RNAi)* worms (*B*). The Lgg1 puncta (asteriscs in *B*) was abundant in the *dnc-1(RNAi)* worms (*B*). (*C*) Co-localization of DsRed and GFP fluorescence in the axonal spheroids (arrows) indicating that the autophagosomes (asteriscs) were accumulated in the axonal spheroids in the *dnc-1(RNAi)* worms. Scale bar = 10 μm (*A–C*).
(TIF)

Figure S3 Pharmacological treatment or starvation did not alter the efficiency of the *dnc-1* knock-down. (*A–D*) The representative image of GFP and *in situ* hybridization against *dnc-1* of ventral cholinergic motor neurons in the *conrol(RNAi)* (*A*) and *dnc-1(RNAi)* (*B*, no treatment; *C*, treated with starvation; *D*, treated with TSA). Scale bars = 10 μm.
(TIF)

Figure S4 Treatment with TSA did not alter the locomotor function or the axonal integrity of the *control(RNAi)* worms. (*A*) Effect of trichostatin A (TSA) on the locomotor function of the *control(RNAi)* worms (n = 35 for each group). (*B, C*) Effect of TSA (100 μM) on the axonal degeneration of the *dnc-1(RNAi)* worms (n = 15 for each group). Statistical analyses were performed using Student's t test.
(TIF)

Movie S1 Representative transport of SNB-1::DsRed puncta (red) in a ventral motor neurons from the control worm.
(MPEG)

Movie S2 Representative transport of SNB-1::DsRed puncta (red) in a ventral motor neurons from the *dnc-1* KD worm.
(MPEG)

Movie S3 Representative transport of Lgg1::DsRed puncta (red) in a primary motor neuron from the control worm.
(MPEG)

Movie S4 Representative transport of Lgg1::DsRed puncta (red) in a primary motor neuron from the *dnc-1* KD worm.
(MPEG)

Movie S5 Representatie transport of Lgg1::DsRed puncta (red) in a ventral motor neurons from the control worm.
(MPEG)

Movie S6 Representatie transport of Lgg1::DsRed puncta (red) in a ventral motor neurons from the *dnc-1* KD worm.
(MPEG)

Materials and Methods S1 Detailed materials and methods for *C. elegans* and human protocols.
(DOCX)

Author Contributions

Conceived and designed the experiments: KI MK FT IM GS. Performed the experiments: KI K. Kawai ZH YI YJ K. Kobayashi TK MW. Analyzed the data: KI K. Kawai MK. Contributed reagents/materials/analysis tools: TK K. Kobayashi IM. Wrote the paper: KI MK FT GS.

References

1. Klionsky DJ, Emr SD (2000) Autophagy as a regulated pathway of cellular degradation. Science 290: 1717–1721.
2. Hara T, Nakamura K, Matsui M, Yamamoto A, Nakahara Y, et al. (2006) Suppression of basal autophagy in neural cells causes neurodegenerative disease in mice. Nature 441: 885–889.
3. Komatsu M, Waguri S, Chiba T, Murata S, Iwata J, et al. (2006) Loss of autophagy in the central nervous system causes neurodegeneration in mice. Nature 441: 880–884.
4. Ravikumar B, Acevedo-Arozena A, Imarisio S, Berger Z, Vacher C, et al. (2005) Dynein mutations impair autophagic clearance of aggregate-prone proteins. Nat Genet 37: 771–776.
5. Komatsu M, Wang QJ, Holstein GR, Friedrich VL Jr., Iwata J, et al. (2007) Essential role for autophagy protein Atg7 in the maintenance of axonal homeostasis and the prevention of axonal degeneration. Proc Natl Acad Sci U S A 104: 14489–14494.
6. Anglade P, Vyas S, Javoy-Agid F, Herrero MT, Michel PP, et al. (1997) Apoptosis and autophagy in nigral neurons of patients with Parkinson's disease. Histol Histopathol 12: 25–31.
7. Sapp E, Schwarz C, Chase K, Bhide PG, Young AB, et al. (1997) Huntingtin localization in brains of normal and Huntington's disease patients. Ann Neurol 42: 604–612.
8. Sasaki S (2011) Autophagy in spinal cord motor neurons in sporadic amyotrophic lateral sclerosis. J Neuropathol Exp Neurol 70: 349–359.
9. Yu WH, Cuervo AM, Kumar A, Peterhoff CM, Schmidt SD, et al. (2005) Macroautophagy--a novel Beta-amyloid peptide-generating pathway activated in Alzheimer's disease. J Cell Biol 171: 87–98.
10. Li L, Zhang X, Le W (2008) Altered macroautophagy in the spinal cord of SOD1 mutant mice. Autophagy 4: 290–293.
11. Yang Y, Xu K, Koike T, Zheng X (2008) Transport of autophagosomes in neurites of PC12 cells during serum deprivation. Autophagy 4: 243–245.
12. Katsumata K, Nishiyama J, Inoue T, Mizushima N, Takeda J, et al. (2010) Dynein- and activity-dependent retrograde transport of autophagosomes in neuronal axons. Autophagy 6: 378–385.
13. Jiang YM, Yamamoto M, Tanaka F, Ishigaki S, Katsuno M, et al. (2007) Gene expressions specifically detected in motor neurons (dynactin 1, early growth response 3, acetyl-CoA transporter, death receptor 5, and cyclin C) differentially correlate to pathologic markers in sporadic amyotrophic lateral sclerosis. J Neuropathol Exp Neurol 66: 617–627.
14. Puls I, Jonnakuty C, LaMonte BH, Holzbaur EL, Tokito M, et al. (2003) Mutant dynactin in motor neuron disease. Nat Genet 33: 455–456.
15. Levy JR, Sumner CJ, Caviston JP, Tokito MK, Ranganathan S, et al. (2006) A motor neuron disease-associated mutation in p150Glued perturbs dynactin function and induces protein aggregation. J Cell Biol 172: 733–745.
16. Laird FM, Farah MH, Ackerley S, Hoke A, Maragakis N, et al. (2008) Motor neuron disease occurring in a mutant dynactin mouse model is characterized by defects in vesicular trafficking. J Neurosci 28: 1997–2005.
17. Katsuno M, Adachi H, Kume A, Li M, Nakagomi Y, et al. (2002) Testosterone reduction prevents phenotypic expression in a transgenic mouse model of spinal and bulbar muscular atrophy. Neuron 35: 843–854.
18. Brenner S (1974) The genetics of Caenorhabditis elegans. Genetics 77: 71–94.
19. Takada T, Iida K, Sasaki H, Taira M, Kimura H (2005) Expression of ADP-ribosylation factor (ARF)-like protein 6 during mouse embryonic development. Int J Dev Biol 49: 891–894.
20. Koushika SP, Schaefer AM, Vincent R, Willis JH, Bowerman B, et al. (2004) Mutations in Caenorhabditis elegans cytoplasmic dynein components reveal specificity of neuronal retrograde cargo. J Neurosci 24: 3907–3916.
21. Kraemer BC, Zhang B, Leverenz JB, Thomas JH, Trojanowski JQ, et al. (2003) Neurodegeneration and defective neurotransmission in a Caenorhabditis elegans model of tauopathy. Proc Natl Acad Sci U S A 100: 9980–9985.
22. Miyara A, Ohta A, Okochi Y, Tsukada Y, Kuhara A, et al. (2011) Novel and Conserved Protein Macoilin Is Required for Diverse Neuronal Functions in Caenorhabditis elegans. PLoS Genet 7: e1001384.
23. Lewis JA, Fleming JT (1995) Basic culture methods. Methods Cell Biol 48: 3–29.
24. Strange K, Christensen M, Morrison R (2007) Primary culture of Caenorhabditis elegans developing embryo cells for electrophysiological, cell biological and molecular studies. Nat Protoc 2: 1003–1012.
25. Stiernagle T (2006) Maintenance of C. elegans. WormBook: 1–11.
26. Paredez AR, Persson S, Ehrhardt DW, Somerville CR (2008) Genetic evidence that cellulose synthase activity influences microtubule cortical array organization. Plant Physiol 147: 1723–1734.
27. Hall DH, Gu G, Garcia-Anoveros J, Gong L, Chalfie M, et al. (1997) Neuropathology of degenerative cell death in Caenorhabditis elegans. J Neurosci 17: 1033–1045.
28. Ishigaki S, Liang Y, Yamamoto M, Niwa J, Ando Y, et al. (2002) X-Linked inhibitor of apoptosis protein is involved in mutant SOD1-mediated neuronal degeneration. J Neurochem 82: 576–584.
29. Katsuno M, Adachi H, Doyu M, Minamiyama M, Sang C, et al. (2003) Leuprorelin rescues polyglutamine-dependent phenotypes in a transgenic mouse model of spinal and bulbar muscular atrophy. Nat Med 9: 768–773.
30. Thomas JH (1990) Genetic analysis of defecation in Caenorhabditis elegans. Genetics 124: 855–872.
31. McIntire SL, Garriga G, White J, Jacobson D, Horvitz HR (1992) Genes necessary for directed axonal elongation or fasciculation in C. elegans. Neuron 8: 307–322.
32. Comley LH, Wishart TM, Baxter B, Murray LM, Nimmo A, et al. (2011) Induction of cell stress in neurons from transgenic mice expressing yellow fluorescent protein: implications for neurodegeneration research. PLoS One 6.
33. Sikorska B, Liberski PP, Giraud P, Kopp N, Brown P (2004) Autophagy is a part of ultrastructural synaptic pathology in Creutzfeldt-Jakob disease: a brain biopsy study. Int J Biochem Cell Biol 36: 2563–2573.
34. Nixon RA, Wegiel J, Kumar A, Yu WH, Peterhoff C, et al. (2005) Extensive involvement of autophagy in Alzheimer disease: an immuno-electron microscopy study. J Neuropathol Exp Neurol 64: 113–122.
35. Mizushima N, Yoshimori T, Levine B (2010) Methods in mammalian autophagy research. Cell 140: 313–326.
36. Melendez A, Levine B (2009) Autophagy in C. elegans. WormBook: 1–26.
37. Ohara S, Ukita Y, Ninomiya H, Ohno K (2004) Axonal dystrophy of dorsal root ganglion sensory neurons in a mouse model of Niemann-Pick disease type C. Exp Neurol 187: 289–298.
38. Noda T, Ohsumi Y (1998) Tor, a phosphatidylinositol kinase homologue, controls autophagy in yeast. J Biol Chem 273: 3963–3966.
39. You YJ, Kim J, Cobb M, Avery L (2006) Starvation activates MAP kinase through the muscarinic acetylcholine pathway in Caenorhabditis elegans pharynx. Cell Metab 3: 237–245.
40. Geeraert C, Ratier A, Pfisterer SG, Perdiz D, Cantaloube I, et al. (2010) Starvation-induced hyperacetylation of tubulin is required for the stimulation of autophagy by nutrient deprivation. J Biol Chem 285: 24184–24194.
41. Morselli E, Maiuri MC, Markaki M, Megalou E, Pasparaki A, et al. (2010) Caloric restriction and resveratrol promote longevity through the Sirtuin-1-dependent induction of autophagy. Cell Death Dis 1: e10.
42. Hansen M, Chandra A, Mitic LL, Onken B, Driscoll M, et al. (2008) A role for autophagy in the extension of lifespan by dietary restriction in C. elegans. PLoS Genet 4: e24.

43. Sarkar S, Krishna G, Imarisio S, Saiki S, O'Kane CJ, et al. (2008) A rational mechanism for combination treatment of Huntington's disease using lithium and rapamycin. Hum Mol Genet 17: 170–178.
44. Harrison DE, Strong R, Sharp ZD, Nelson JF, Astle CM, et al. (2009) Rapamycin fed late in life extends lifespan in genetically heterogeneous mice. Nature 460: 392–395.
45. Robida-Stubbs S, Glover-Cutter K, Lamming DW, Mizunuma M, Narasimhan SD, et al. (2012) TOR signaling and rapamycin influence longevity by regulating SKN-1/Nrf and DAF-16/FoxO. Cell Metab 15: 713–724.
46. Reed NA, Cai D, Blasius TL, Jih GT, Meyhofer E, et al. (2006) Microtubule acetylation promotes kinesin-1 binding and transport. Curr Biol 16: 2166–2172.
47. Dompierre JP, Godin JD, Charrin BC, Cordelieres FP, King SJ, et al. (2007) Histone deacetylase 6 inhibition compensates for the transport deficit in Huntington's disease by increasing tubulin acetylation. J Neurosci 27: 3571–3583.
48. Akella JS, Wloga D, Kim J, Starostina NG, Lyons-Abbott S, et al. (2010) MEC-17 is an alpha-tubulin acetyltransferase. Nature 467: 218-222.
49. Ori-McKenney KM, Xu J, Gross SP, Vallee RB (2010) A cytoplasmic dynein tail mutation impairs motor processivity. Nat Cell Biol 12: 1228–1234.
50. Ross JL, Wallace K, Shuman H, Goldman YE, Holzbaur EL (2006) Processive bidirectional motion of dynein-dynactin complexes in vitro. Nat Cell Biol 8: 562–570.
51. Haghnia M, Cavalli V, Shah SB, Schimmelpfeng K, Brusch R, et al. (2007) Dynactin is required for coordinated bidirectional motility, but not for dynein membrane attachment. Mol Biol Cell 18: 2081–2089.
52. Welte MA (2010) Bidirectional transport: matchmaking for motors. Curr Biol 20: R410–413.
53. Caccamo A, Majumder S, Deng JJ, Bai Y, Thornton FB, et al. (2009) Rapamycin rescues TDP-43 mislocalization and the associated low molecular mass neurofilament instability. J Biol Chem 284: 27416–27424.
54. Spilman P, Podlutskaya N, Hart MJ, Debnath J, Gorostiza O, et al. (2010) Inhibition of mTOR by rapamycin abolishes cognitive deficits and reduces amyloid-beta levels in a mouse model of Alzheimer's disease. PLoS One 5: e9979.
55. Zhang X, Li L, Chen S, Yang D, Wang Y, et al. (2011) Rapamycin treatment augments motor neuron degeneration in SOD1 (G93A) mouse model of amyotrophic lateral sclerosis. Autophagy 7.

OPEN ACCESS

RESEARCH PAPER

Clinical features and a mutation with late onset of limb girdle muscular dystrophy 2B

Toshiaki Takahashi,[1] Masashi Aoki,[2] Naoki Suzuki,[2] Maki Tateyama,[2] Chikako Yaginuma,[3] Hitomi Sato,[3] Miho Hayasaka,[3,4] Hitomi Sugawara,[3] Mariko Ito,[3,5] Emi Abe-Kondo,[3,6] Naoko Shimakura,[2] Tohru Ibi,[7,8] Satoshi Kuru,[9] Tadashi Wakayama,[9,10] Gen Sobue,[11] Naoki Fujii,[12] Toshio Saito,[13] Tsuyoshi Matsumura,[13] Itaru Funakawa,[14] Eiichiro Mukai,[15] Toru Kawanami,[16] Mitsuya Morita,[17] Mineo Yamazaki,[18] Takashi Hasegawa,[19,20] Jun Shimizu,[21] Shoji Tsuji,[21] Shigeki Kuzuhara,[22,23] Hiroyasu Tanaka,[1] Masaru Yoshioka,[1,3] Hidehiko Konno,[1] Hiroshi Onodera,[1] Yasuto Itoyama[2,24]

► Additional supplementary files are published online only. To view these files please visit the journal online (http://dx.doi.org/10.1136/jnnp-2011-301339).

For numbered affiliations see end of article

Correspondence to
Dr M Aoki, Department of Neurology, Tohoku University School of Medicine, 1-1 Seiryo-machi, Sendai 980-8574, Japan; aokim@med.tohoku.ac.jp

Received 2 September 2011
Revised 18 April 2012
Accepted 13 May 2012
Published Online First 15 December 2012

ABSTRACT

Objective and methods Dysferlin encoded by *DYSF* deficiency leads to two main phenotypes, limb girdle muscular dystrophy (LGMD) 2B and Miyoshi myopathy. To reveal in detail the mutational and clinical features of LGMD2B in Japan, we observed 40 Japanese patients in 36 families with LGMD2B in whom dysferlin mutations were confirmed.

Results and conclusions Three mutations (c.1566C>G, c.2997G>T and c.4497delT) were relatively more prevalent. The c.2997G>T mutation was associated with late onset, proximal dominant forms of dysferlinopathy, a high probability that muscle weakness started in an upper limb and lower serum creatine kinase (CK) levels. The clinical features of LGMD2B are as follows: (1) onset in the late teens or early adulthood, except patients homozygous for the c.2997G>T mutation; (2) lower limb weakness at onset; (3) distal change of lower limbs on muscle CT at an early stage; (4) impairment of lumbar erector spinal muscles on muscle CT at an early stage; (5) predominant involvement of proximal upper limbs; (6) preservation of function of the hands at late stage; (7) preservation of strength in neck muscles at late stage; (8) lack of facial weakness or dysphagia; (9) avoidance of scoliosis; (10) hyperCkaemia; (11) preservation of cardiac function; and (12) a tendency for respiratory function to decline with disease duration. It is important that the late onset phenotype is found with prevalent mutations.

INTRODUCTION

Dysferlinopathies are autosomal recessive muscular dystrophies caused by mutations in the dysferlin gene (*DYSF*, MIM# 603009). Dysferlin deficiency leads to two main phenotypes: limb girdle muscular dystrophy (LGMD) 2B and Miyoshi myopathy (MM).[1 2] Dysferlin is located on the plasma membrane of skeletal muscle and is deficient in patients with MM and LGMD2B.[3 4] However, atypical immunostaining in muscle from patients with dysferlin mutations occurs,[5 6] and dysferlin expression is not normal in sarcoglycanopathy, dystrophinopathy,[7] caveolinopathy[8 9] or calpainopathy[6] muscles. Therefore, the final diagnosis of dysferlinopathy requires identification of mutations in the dysferlin gene. We first reported dysferlin mutations in Japanese patients with MM[10] and in a patient from a non-European ethnic group with distal anterior compartment myopathy (DACM),[11] a relatively new phenotype of dysferlinopathy.[12] Furthermore, we revealed that, in MM, four mutations (c.1566C>G, c.2997G>T, c.3373delG and c.4497delT) were relatively more prevalent in the Japanese population and the c.2997G>T mutation was associated with late onset.[13] Although mutation analysis of the dysferlin gene is a time consuming task because of the large size of the gene,[14] large series of patients with dysferlin gene mutations have been studied.[6 15–24] However, few detailed analyses of the clinical features of LGMD2B, especially in relation to various types of mutations, have been reported. Here we report the clinical features of a series of 40 patients in 36 families with LGMD2B in whom dysferlin mutations were confirmed, and cardiac and respiratory functions were involved. In particular, we took into account the duration that had elapsed since onset when the clinical data were examined.

MATERIALS AND METHODS

We retrospectively observed 40 Japanese patients in 36 families with LGMD2B in whom dysferlin mutations were confirmed. LGMD was defined as symptomatic myopathy excluding MM and DACM at the first visit to a neurologist. Mutational analysis was performed by single strand conformation polymorphism analysis and sequencing on genomic DNA using our previously reported method,[13 14 25] with minor modifications (Ref Seq NM_003494.2), and with informed consent and approval of our local ethics committee. We retrospectively reassessed the history of onset and progression of the disease. The clinical examination included manual muscle testing using the Medical Research Council (MRC) Scale and assignment of scales for the proximal limb muscles, as proposed by Brooke *et al*.[26] Clinical examination was carried out by neurologists from the study groups for muscular dystrophy in Japan.

Most patients had undergone muscle CT scans at some stage of the disease. Serum creatine kinase (CK) activity was measured. Cardiac and respiratory functions were evaluated. We selected the first and last manual muscle testing data and the last data on the scales for the proximal limb muscles, CK activity, cardiac function and respiratory function. We used all muscle CT scans. Patients were divided into three groups according to whether they had the homozygous c.2997G>T (p.Trp999Cys) mutation, the heterozygous c.2997G>T (p.Trp999Cys) mutation or other mutations. Difference in age at onset among the groups was evaluated by the Kruskal–Wallis test. Multiple comparison of age at onset between each group was assessed by Scheffé's F test. Difference in the first symptom among the groups was evaluated by the χ^2 for independence test. Kaplan–Meier curves with log rank test were used to examine survival at each milestone of progression in the groups. Pearson's correlation coefficient test was used to identify significant associations in ejection fraction (EF) (n=21), atrial natriuretic peptide (n=9), brain natriuretic peptide (n=7), per cent vital capacity (%VC) (n=23), carbon dioxide partial pressure (pCO_2) (n=16) and oxygen partial pressure (pO_2) (n=16) with disease duration. Because supine and standing position chest x-rays were mingled, Pearson's correlation coefficient test was not used for the cardiothoracic ratio (n=22).

RESULTS

Mutations

We identified 17 different mutations in 36 families (table 1). Two mutations (c.2974T>C (p.Trp992Arg) and c.2997G>T (p.Trp999Cys)) were missense mutations and four mutations (c.342+1G>A, c.937+1G>A, c.2643+1G>A and c.4794 +1G>A) were splice site mutations. The others were nonsense mutations. The c.2997G>T (p.Trp999Cys) mutation was present in 26 alleles (36.1%). The c.1566C>G (p.Tyr522X) mutation and the c.4497delT mutation were both present in eight alleles (11.1%). We identified the c.3373delG mutation that has high frequency in Japanese patients with MM[13] in only one allele.

Clinical course

Mean age at onset of all patients was 26.6±9.9 years (range 14–58): the group homozygous for the c.2997G>T (p.Trp999Cys) mutation, 37.9±10.2 years (19–58); the group heterozygous for the c.2997G>T (p.Trp999Cys) mutation, 26.8 ±7.6 years (14–35); and the group without the c.2997G>T (p.Trp999Cys) mutation, 21.8±5.8 years (14–41). The difference between the group homozygous for the c.2997G>T (p.Trp999Cys) mutation and the group heterozygous for the c.2997G>T (p.Trp999Cys) mutation was significant ($p<0.05$). The difference between the group homozygous for the c.2997G>T (p.Trp999Cys) mutation and the group without the c.2997G>T (p.Trp999Cys) mutation was significant ($p<0.01$) (figure 1). The first symptom in most patients was lower limb weakness. Walking on tiptoe was the first sign in one patient. In three patients with the homozygous c.2997G>T (p.Trp999Cys) mutation, the first symptom was upper limb weakness. In two patients, one of them carrying the homozygous c.2997G>T (p.Trp999Cys) mutation, upper limb weakness was concomitant with lower limb weakness. There was a significant difference ($p<0.01$) in the probability that the first symptom was upper limb weakness among these three groups. The first symptom in one patient was left brachial pain and in another patient it was limitation of the elbow, hip, knee and spine.[27] In the early stage of the clinical course, hypertrophy of the calves was noticed in three patients. Winged scapula, rigid spine[27] and hollow foot were observed in one patient each. Lordosis was observed in two patients. Weakness of the face, dysphagia, scoliosis and kyphosis were not found. Choreic movements and pollakisuria were found in one patient.[28] Mean duration at difficulty in running was 1.3 years from disease onset (range 0–10), 3.1 years (0–14) for difficulty in climbing stairs, 5.5 years (0–16) for stumbling, 6.0 years (0–10) for difficulty in standing on tiptoe, 6.7 years (0–15) for rising from the floor, 8.7 years (0–25) for noticing weakness in a proximal upper limb, 12.5 years (3–23) for walking with a cane, 20.4 years (9–35) for noticing weakness in a distal upper limb, 21.6 years (13–29) for using a wheelchair and 31.0 years (16–45) for using an electric wheelchair. There was a significant difference ($p<0.05$) in the survival ratio only at the stage of difficulty in standing on tiptoe among these three groups (figure 2). There were no significant differences in survival at the stage of the other symptoms between these three groups. According to the scales for the proximal limb muscles, only two patients each reached the severest stage of arms and shoulders (cannot raise hands to mouth and have no useful function) and hips and legs (confined to bed).

Manual muscle testing

In the first decade of the disease, the muscles of the lower limbs were predominantly involved. In the upper limbs, the deltoid muscle was predominantly involved. In the second decade of the disease, the biceps and triceps brachii muscles became weak. Later on, the flexor and extensor of the hand became weak. Muscle weakness progressed and, in the fifth decade of the disease, the muscles of the lower limbs were very weak (1 on the MRC Scale). In the patient with 52 years of disease duration, although the muscles of the upper and the lower limbs were 0 on the MRC scale, the flexor and extensor of the neck were relatively preserved (2 on the MRC Scale).

Muscle CT scans

The CT scans revealed low density changes in the gastrocnemius, especially in the medial heads, soleus, hamstrings and the erector spinal group, which was mainly affected in the lateral parts in the early disease stage. Low density abnormalities in the quadriceps femoris and the adductor magnus muscles were observed at close to 10 years after disease onset. The tibialis anterior, the peroneal group, the gluteal group, the quadrates lumborum and the deltoid muscles were involved at 10 years after onset. The gracilis and sarcorius muscles were preserved and had hypertrophied during the second decade of disease duration. Approximately 20 years after disease onset, low density changes in the dorsal muscles occurred in the neck region, particularly in the transversospinal group, except for the semispinalis capitis muscle. All muscles were replaced by low density tissue or were atrophied at 30 years after disease onset. The gluteal group, the psoas major muscle, the lateral abdominal group and the levator scapulae muscle were preserved in the late stage. There were exceptional cases. In one patient, low density changes in the dorsal muscles in the neck region occurred at an early stage. In another patient, the quadriceps femoris muscles were more severely damaged than the hamstrings at 14 years of disease duration.

Serum CK levels

Although serum CK levels were very high, there was a tendency for levels to decrease with disease duration (figure 3). There was a trend in the distribution of the levels by

Table 1 Summary of dysferlin gene mutations of patients in this study

Patient	Sex	Age (years)	Disease duration (years)	Exon	Nucleotide change	Protein change	State
Dys48-1	M	54	23	28	c.2997G>T	p.Trp999Cys	Homozygous
Dys58-1	F	51	8	28	c.2997G>T	p.Trp999Cys	Homozygous
Dys64-1	M	58	19	28	c.2997G>T	p.Trp999Cys	Homozygous
Dys93-1	F	57	17	28	c.2997G>T	p.Trp999Cys	Homozygous
Dys99-1	F	55	11	28	c.2997G>T	p.Trp999Cys	Homozygous
Dys106-1	F	22	3	28	c.2997G>T	p.Trp999Cys	Homozygous
Dys113-1	M	57	17	28	c.2997G>T	p.Trp999Cys	Homozygous
Dys123-1	F	59	25	28	c.2997G>T	p.Trp999Cys	Homozygous
Dys133-1	M	66	8	28	c.2997G>T	p.Trp999Cys	Homozygous
Dys170-1	F	38	7	28	c.2997G>T	p.Trp999Cys	Homozygous
Dys13-1	M	43	29	28 34	c.2997G>T c.3771G>A	p.Trp999Cys p.Trp1257X	Compound heterozygous
Dys55-1	F	47	22	28 37	c.2997G>T c.3959_3960insA	p.Trp999Cys p.Met1320IlefsX26	Compound heterozygous
Dys114-1	M	50	15	Intron 25 28	c.2643+1G>A c.2997G>T	Splice site p.Trp999Cys	Compound heterozygous
Dys120-1	M	55	25	18 28	c.1566C>G c.2997G>T	p.Tyr522X p.Trp999Cys	Compound heterozygous
Dys124-1	F	36	12	18 28	c.1566C>G c.2997G>T	p.Tyr522X p.Trp999Cys	Compound heterozygous
Dys127-1	F	56	23	18 28	c.1566C>G c.2997G>T	p.Tyr522X p.Trp999Cys	Compound heterozygous
4	M	75	49	Intron 25 41	c.2643+1G>A c.4497delT	Splice site p.Phe1499LeufsX4	Compound heterozygous
5	M	Died at 59	Died at 42	21	c.1958delG	p.Gly653ValfsX3	Homozygous
15	F	50	34	37	c.3959_3960insA	p.Met1320IlefsX26	Homozygous
39	F	74	52	Intron 25	c.2643+1G>A	Splice site	Homozygous
44	M	41	14	29 41	c.3112C>T c.4497delT	p.Arg1038X p.Phe1499LeufsX4	Compound heterozygous
47	M	55	37	37	c.3959_3960insA	p.Met1320IlefsX26	Homozygous
Dys37-1	M	60	40	Intron 10	c.937+1G>A	Splice site	Homozygous
Dys37-2	F	51	24	Sister of Dys37-1			
Dys43-1	F	36	19	18	c.1566C>G	p.Tyr522X	Homozygous
Dys43-2	F	35	21	Sister of Dys43-1			
Dys46-1	F	67	48	41	c.4497delT	p.Phe1499LeufsX4	Homozygous
Dys50-2	M	70	29	41	c.4497delT	p.Phe1499LeufsX4	Homozygous
Dys59-1	F	49	27	28	c.2974T>C	p.Trp992Arg	Homozygous
Dys61-1	F	43	21	41	c.4497delT	p.Phe1499LeufsX4	Homozygous
Dys78-1	F	54	30	Intron 10	c.937+1G>A	Splice site	Homozygous
Dys84-1	F	64	45	14	c.1321C>T	p.Gln441X	Homozygous
Dys84-2	M	52	32	Brother of Dys84-1			
Dys89-1	F	68	40	18 28	c.1566C>G c.2974T>C	p.Tyr522X p.Trp992Arg	Compound heterozygous
Dys117-1	M	32	9	18	c.1566C>G	p.Tyr522X	Homozygous
Dys117-2	M	30	16	Brother of Dys117-1			
Dys126-1	M	23	2	Intron 4 54	c.342+1G>A c.6135G>A	Splice site p.Trp2045X	Compound heterozygous
Dys145-1	F	27	10	6	c.610C>T	p.Arg204X	Homozygous
Dys146-1	F	58	34	31 Intron 43	c.3373delG c.4794+1G>A	p.Glu1125LysfsX9 splice site	Compound heterozygous
Dys163-1	M	36	11	6	c.493delC	p.Leu165SerfsX48	Homozygous

c.2997G>T (p.Trp999Cys) mutation. Levels in the group homozygous for the c.2997G>T (p.Trp999Cys) mutation were lower than those of the other two groups.

Cardiac function

Although supine and standing position chest x-rays were mingled, in half of the patients the cardiothoracic ratio was >50%. No significant correlation was observed between EF and disease duration. Except for two patients, levels of EF were >50%. In all the patients, concentrations of atrial natriuretic peptide were within the normal range. Except for one patient, concentrations of brain natriuretic peptide were within the normal range. No significant correlation was observed between these peptides and disease duration. Although 19 patients

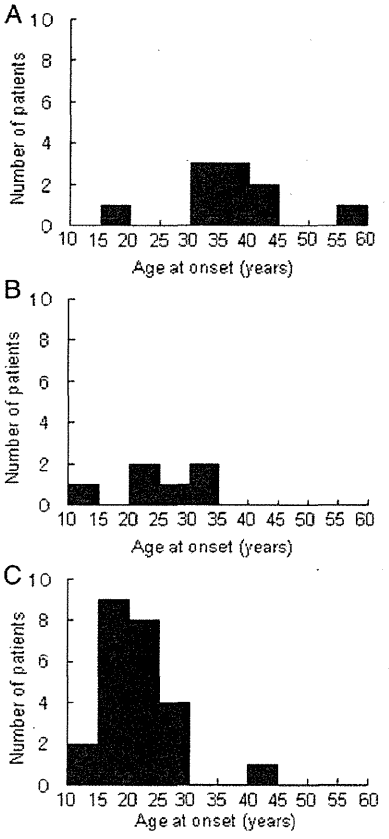

Figure 1 Histogram by age at onset. (A) Patients homozygous for the c.2997G>T mutation. (B) Patients heterozygous for the c.2997G>T mutation. (C) Patients without the c.2997G>T mutation.

exhibited normal findings on ECG, abnormalities were found in nine patients. The ECG showed premature ventricular contraction in one patient, one degree atrioventricular block in two patients, incomplete right bundle branch block in two patients, left axis deviation in two patients, left atrial hypertrophy in one patient, right ventricular hypertrophy in three patients, left ventricular hypertrophy in three patients, ST change in two patients and negative T in one patient.

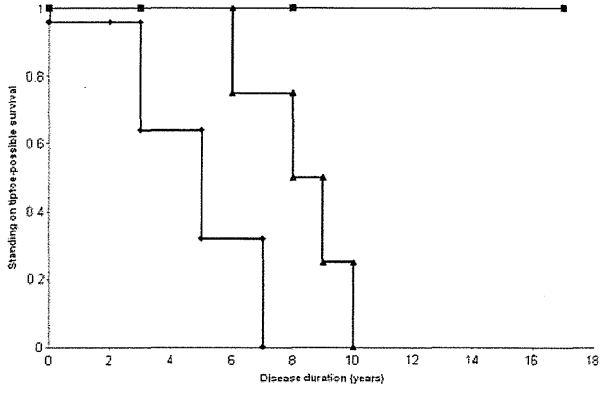

Figure 2 Standing on tiptoe—possible survival curve. Survival curve of patients homozygous for the c.2997G>T mutation (line with squares), those heterozygous for the c.2997G>T mutation (line with triangles) and those without the c.2997G>T mutations (line with diamonds).

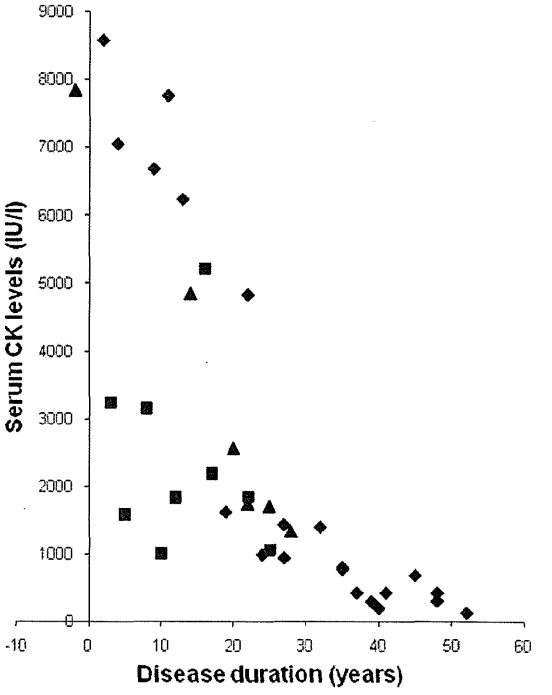

Figure 3 Serum creatine kinase (CK) levels during the disease course. Levels of serum CK in patients homozygous for the c.2997G>T mutation (squares), heterozygous for the c.2997G>T mutation (triangles) and those without the c.2997G>T mutations (diamonds).

Respiratory function

A statistically significant ($p<0.01$) correlation ($r=-0.545$) was observed between %VC and disease duration (figure 4). In 48% of patients, %VC was <80%. Although no significant correlation was observed between pCO_2 and disease duration, in 44% of patients, levels of pCO_2 were >45 mm Hg. In most patients, levels of pO_2 were >70 mm Hg. No significant correlation was observed between pO_2 and disease duration. Four patients had

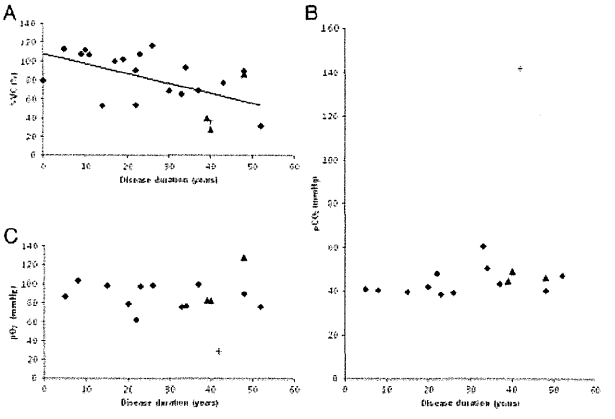

Figure 4 Respiratory function. (A) Per cent vital capacity (%VC) according to disease duration. The line is the regression line of %VC and disease duration. (B) Carbon dioxide partial pressure (pCO_2) according to disease duration. (C) Oxygen partial pressure (pO_2) according to disease duration. The triangles indicate levels in patients who had used non-invasive positive pressure ventilation. The cross (+) indicates the level in a patient who died after 42 years of disease duration of respiratory failure.

used non-invasive positive pressure ventilation (NIPPV). One patient who used NIPPV died after 42 years of disease duration from respiratory failure.

DISCUSSION

Three mutations (c.2997G>T (p.Trp999Cys), c.1566C>G (p.Tyr522X) and c.4497delT) were relatively more prevalent in the present Japanese patients with LGMD2B. Also, in Japanese patients with MM, these three mutations were relatively more prevalent in our previous study.[13] We identified the c.3373delG mutation that occurred with high frequency in Japanese patients with MM, as well as these three mutations,[13] in only one allele in Japanese patients with LGMD2B.

In MM, patients with the c.2997G>T (p.Trp999Cys) mutation had a significantly late onset.[13] Tagawa *et al*[6] reported that age of onset in patients homozygous for the c.2997G>T (p.Trp999Cys) mutation was later than the third decade of life. In this study, especially in patients homozygous for the c.2997G>T (p.Trp999Cys) mutation, onset was significantly late. Only 10% of patients homozygous for the c.2997G>T (p.Trp999Cys) mutation developed muscle symptoms by 30 years. In contrast, 90% of patients without this mutation developed muscle symptoms by the same age. However, it is difficult to explain why the c.2997G>T (p.Trp999Cys) mutation is related to late onset forms. In an immunohistochemical analysis by Tagawa *et al*,[6] although one patient with the homozygous c.2997G>T mutation (p.Trp999Cys) showed an 'abnormal' pattern, cytoplasmic accumulation of immunopositive material with deficiency of membrane staining or positive/negative mosaic membrane staining, three patients with the same mutation showed a negative pattern. Guglieri *et al*[21] reported that patients carrying two truncating mutations showed the first muscular symptoms earlier in life than subjects harbouring double missense substitutions. Indeed, the c.2997G>T mutation is theoretically deduced to be a missense mutation (p.Trp999Cys). Meanwhile, in this study, there were only two patients carrying missense mutations other than the c.2997G>T (p.Trp999Cys) mutation. Thus it is difficult to discuss statistically whether an association between the c.2997G>T (p.Trp999Cys) mutation and late onset forms is due to a missense mutation or other inherent characteristics. Nonetheless, it is important that the late onset phenotype is found with prevalent mutations.

Although patients homozygous for the c.2997G>T (p.Trp999Cys) mutation had late onset, no difference in progression was observed in those harbouring the c.2997G>T (p.Trp999Cys) mutation, except for difficulty in standing on tiptoe. This suggests that the c.2997G>T (p.Trp999Cys) mutation is related to late onset but not to the slow progression of the disease. Furthermore, the c.2997G>T (p.Trp999Cys) mutation may be relevant to the proximal dominant impairment in dysferlinopathy, diagnosed as the limb girdle type. Interestingly, there was only one patient homozygous for the c.2997G>T (p.Trp999Cys) mutation in 27 families with MM.[13] Moreover, patients homozygous for the c.2997G>T (p.Trp999Cys) mutation had a high probability that the muscle weakness started in the upper limbs. In addition, serum CK levels in patients homozygous for the c.2997G>T (p.Trp999Cys) mutation were lower than those in the other two groups.

We investigated the clinical features of 40 patients in 36 families with LGMD2B in whom dysferlin mutations were confirmed. Disease duration was long (26.6±9.9 years) in this study. The clinical features of LGMD2B in this study were as follows: (1) onset in the late teens or early adulthood except in patients homozygous for the c.2997G>T (p.Trp999Cys) mutation; (2) lower limb weakness at onset in most patients; (3) distal change of lower limbs on muscle CT in the early stage; (4) impairment of lumbar erector spinal muscles on muscle CT in the early stage; (5) predominant involvement of the proximal upper limbs; (6) preservation of function of the hands in late stage; (7) preservation of strength in the neck muscles in late stage; (8) lack of facial weakness or dysphagia; (9) avoidance of scoliosis; (10) hyper-Ckaemia; (11) preservation of cardiac function; and (12) tendency for respiratory function to decline with disease duration and occasional necessity for ventilatory assistance.

Age at onset was similar to that reported for various types of mutations.[18 19 21] However, patients with disease onset at 73 years[24 29] or congenital onset[30] have been reported. Clinicians may not have taken into account analyses of the dysferlin gene for such patients.

Nishida *et al* proposed the name 'distal limb girdle type muscular dystrophy' for patients with MM that develop proximal muscle involvement relatively early.[31 32] Nguyen *et al*[17] classified patients for whom it was not possible to distinguish between a distal phenotype of MM and a limb girdle phenotype, even when examined at onset, as a distinct 'proximodistal' phenotype group. Although patients with the typical features of MM[13 33] or asymptomatic hyper-CKaemia were excluded from the present study, variable patterns of weakness in the lower limbs were observed, as in previous studies.[17 19 20 22 24] However, the predominant muscle weakness was in proximal sites of the upper limbs in the present study.

The results of muscle CT scan in this study were similar to those of detailed imaging studies in LGMD2B at a relatively early stage.[23 34 35] In this study, we had only one case in whom a low density change in the dorsal muscle in the neck region occurred in the early stage. In contrast, two patients showed fatty muscle degeneration of the cervical elector spinae muscles after 9 or 10 years of disease duration, in a study performed using 3.0 T MRI.[35] Another exceptional finding was a case in which the quadriceps femoris muscles were more severely damaged than the hamstrings, which was reported in two of five patients.[34]

In the present study, only two patients showed levels of EF that were <50% and the patient who showed the lowest EF (32.7%) had no symptoms or signs of cardiomyopathy.[36] Guglieri *et al*[21] reported cardiac rhythm changes in three patients and left ventricular hypertrophy in four patients from a total of 22 LGMD2B patients. Wenzel *et al*[37] reported ECG abnormalities (repolarisation abnormalities or left ventricular hypertrophy) in four patients and pathological echocardiographic parameters in five of seven LGMD2B patients. Furthermore, two patients had symptoms and signs of dilated cardiomyopathy. Choi *et al*[38] reported left ventricular hypertrophy on ECG in two patients, no cardiac signs in one patient and mildly decreased EF (45%) in one patient among five MM patients. Therefore, we think that in most patients with LGMD2B, in spite of the existence of laboratorial abnormalities, cardiac function was clinically preserved.

Mahjneh *et al*[16] reported that patients with LGMD2B with disease durations of up to 7 years might show slight restrictive lung disease. Cagliani *et al*[39] reported that respiratory tests showed mild obstructive signs at the small airways in a 20-year-old man with LGMD2B. Illa *et al*[12] reported that pulmonary function tests revealed a mild reduction in VC in two

patients with DACM. In this study, many patients showed pathological levels of respiratory parameters and levels of %VC decreased with disease duration. Furthermore, some patients needed NIPPV and one patient died of respiratory failure. The change in muscles related to respiratory function worsens with disease duration. Therefore, it is important to pay attention to respiratory function in patients with dysferlinopathy.

Author affiliations
[1]Department of Neurology and Division of Clinical Research, National Hospital Organization Nishitaga National Hospital, Sendai, Japan
[2]Department of Neurology, Tohoku University School of Medicine, Sendai, Japan
[3]Department of Clinical Laboratory and Division of Clinical Research, National Hospital Organization Nishitaga National Hospital, Sendai, Japan
[4]Department of Clinical Laboratory, National Hospital Organization Fukushima National Hospital, Fukushima, Japan
[5]Department of Clinical Laboratory, National Hospital Organization Sendai Medical Centre, Sendai, Japan
[6]Department of Clinical Laboratory, Sagami Hospital of Rehabilitation, Sagamihara, Japan
[7]Department of Neurology, Aichi Medical University, Aichi, Japan
[8]Division of Pathophysiology and Therapeutics, College of Nursing, Aichi Medical University, Aichi, Japan
[9]Department of Neurology, National Hospital Organization Suzuka National Hospital, Mie, Japan
[10]Dr Wakayama's office, Nagoya, Japan
[11]Department of Neurology, Nagoya University Graduate School of Medicine, Nagoya, Japan
[12]Department of Neurology, National Hospital Organization Omuta National Hospital, Fukuoka, Japan
[13]Department of Neurology, National Hospital Organization Toneyama National Hospital, Osaka, Japan
[14]Department of Neurology, National Hospital Organization Hyogo-Cyuo National Hospital, Hyogo, Japan
[15]Department of Neurology, National Hospital Organization Nagoya Medical Centre, Nagoya, Japan
[16]Division of Neurology, Third Department of Internal Medicine, Yamagata University Faculty of Medicine, Yamagata, Japan
[17]Division of Neurology, Department of Internal Medicine, Jichi Medical University, Tochigi, Japan
[18]Division of Neurology, Department of Internal Medicine, Nippon Medical School, Tokyo, Japan
[19]Division of Neurology, Department of Internal Medicine, Jikei University School of Medicine, Tokyo, Japan
[20]Department of Internal Medicine, Asao General Hospital of Rehabilitation, Kawasaki, Japan
[21]Department of Neurology, Graduate School of Medicine, University of Tokyo, Tokyo, Japan
[22]Department of Neurology, Mie University School of Medicine, Mie, Japan
[23]Department of Medical Welfare, Suzuka University of Medical Science Faculty of Health Science, Mie, Japan
[24]National Centre Hospital, National Centre of Neurology and Psychiatry, Tokyo, Japan

Acknowledgements The authors thank the patients for participating in the study, Dr Mitsuru Kawai, National Hospital Organisation East Saitama National Hospital, for providing advice and Mr Brent Bell for reading the manuscript.

Contributors TT designed the study, conducted the mutational analysis, analysed the data, and drafted and revised the paper. MA supervised the study and revised the paper. NSu analysed the data, and drafted and revised the draft paper. MT analysed the data and revised the draft paper. CY, HSa, MH, HSu, MI, EA-K and NSh performed the mutational analysis and revised the draft paper. TI, SKur, TW, GS, NF, TS, TM, IF, EM, TK, MM, MYa, TH, JS, ST, SKuz and HT analysed the data and revised the draft paper. MYo, HK, HO and YI supervised the study and revised the draft paper.

Funding This work was supported by Intramural Research Grants (20B-12, 20B-13, 23-4 and 23-5) for Neurological and Psychiatric Disorders of NCNP.

Competing interests None.

Patient consent Obtained.

Ethics approval The study was approved by the National Hospital Organisation Nishitaga National Hospital and Tohoku University School of Medicine.

Provenance and peer review Not commissioned; externally peer reviewed.

REFERENCES

1. **Liu J,** Aoki M, Illa I, *et al*. Dysferlin, a novel skeletal muscle gene, is mutated in Miyoshi myopathy and limb girdle muscular dystrophy. *Nat Genet* 1998;**20**:31–6.
2. **Bashir R,** Britton S, Strachan T, *et al*. A gene related to Caenorhabditis elegans spermatogenesis factor fer-1 is mutated in limb-girdle muscular dystrophy type 2B. *Nat Genet* 1998;**20**:37–42.
3. **Anderson LV,** Davison K, Moss JA, *et al*. Dysferlin is a plasma membrane protein and is expressed early in human development. *Hum Mol Genet* 1999;**8**:855–61.
4. **Matsuda C,** Aoki M, Hayashi YK, *et al*. Dysferlin is a surface membrane-associated protein that is absent in Miyoshi myopathy. *Neurology* 1999;**53**:1119–22.
5. **Saito A,** Higuchi I, Nakagawa M, *et al*. Miyoshi myopathy patients with novel 5' splicing donor site mutations showed different dysferlin immunostaining at the sarcolemma. *Acta Neuropathol* 2002;**104**:615–20.
6. **Tagawa K,** Ogawa M, Kawabe K, *et al*. Protein and gene analyses of dysferlinopathy in a large group of Japanese muscular dystrophy patients. *J Neurol Sci* 2003;**211**:23–8.
7. **Piccolo F,** Moore SA, Ford GC, *et al*. Intracellular accumulation and reduced sarcolemmal expression of dysferlin in limb-girdle muscular dystrophies. *Ann Neurol* 2000;**48**:902–12.
8. **Matsuda C,** Hayashi YK, Ogawa M, *et al*. The sarcolemmal proteins dysferlin and caveolin-3 interact in skeletal muscle. *Hum Mol Genet* 2001;**10**:1761–6.
9. **Tateyama M,** Aoki M, Nishino I, *et al*. Mutation in the caveolin-3 gene causes a peculiar form of distal myopathy. *Neurology* 2002;**58**:323–5.
10. **Matsumura T,** Aoki M, Nagano A, *et al*. Molecular genetic analysis of dysferlin in Japanese patients with Miyoshi myopathy. *Proc Japan Acad* 1999;**75**,Ser. B:207–12.
11. **Saito H,** Suzuki N, Ishiguro H, *et al*. Distal anterior compartment myopathy with early ankle contractures. *Muscle Nerve* 2007;**36**:525–7.
12. **Illa I,** Serrano-Munuera C, Gallardo E, *et al*. Distal anterior compartment myopathy: a dysferlin mutation causing a new muscular dystrophy phenotype. *Ann Neurol* 2001;**49**:130–4.
13. **Takahashi T,** Aoki M, Tateyama M, *et al*. Dysferlin mutations in Japanese Miyoshi myopathy: relationship to phenotype. *Neurology* 2003;**60**:1799–804.
14. **Aoki M,** Liu J, Richard I, *et al*. Genomic organization of the dysferlin gene and novel mutations in Miyoshi myopathy. *Neurology* 2001;**57**:271–8.
15. **Argov Z,** Sadeh M, Mazor K, *et al*. Muscular dystrophy due to dysferlin deficiency in Libyan Jews. Clinical and genetic features. *Brain* 2000;**123**:1229–37.
16. **Mahjneh I,** Marconi G, Bushby K, *et al*. Dysferlinopathy (LGMD2B): a 23-year follow-up study of 10 patients homozygous for the same frameshifting dysferlin mutations. *Neuromuscul Disord* 2001;**1**:20–6.
17. **Nguyen K,** Bassez G, Bernard R, *et al*. Dysferlin mutations in LGMD2B, Miyoshi myopathy, and atypical dysferlinopathies. *Hum Mutat* 2005;**26**:165.
18. **Cagliani R,** Magri F, Toscano A, *et al*. Mutation finding in patients with dysferlin deficiency and role of the dysferlin interacting proteins annexin A1 and A2 in muscular dystrophies. *Hum Mutat* 2005;**26**:283.
19. **Nguyen K,** Bassez G, Krahn M, *et al*. Phenotypic study in 40 patients with dysferlin gene mutations: high frequency of atypical phenotypes. *Arch Neurol* 2007;**64**:1176–82.
20. **Leshinsky-Silver E,** Argov Z, Rozenboim L, *et al*. Dysferlinopathy in the Jews of the Caucasus: a frequent mutation in the dysferlin gene. *Neuromuscul Disord* 2007;**17**:950–4.
21. **Guglieri M,** Magri F, D'Angelo MG, *et al*. Clinical, molecular, and protein correlations in a large sample of genetically diagnosed Italian limb girdle muscular dystrophy patients. *Hum Mutat* 2008;**29**:258–66.
22. **Krahn M,** Béroud C, Labelle V, *et al*. Analysis of the DYSF mutational spectrum in a large cohort of patients. *Hum Mutat* 2009;**30**:E345–75.
23. **Paradas C,** Llauger J, Diaz-Manera J, *et al*. Redefining dysferlinopathy phenotypes based on clinical findings and muscle imaging studies. *Neurology* 2010;**75**:316–23.
24. **Klinge L,** Aboumousa A, Eagle M, *et al*. New aspects on patients affected by dysferlin deficient muscular dystrophy. *J Neurol Neurosurg Psychiatry* 2010;**81**:946–53.
25. **Aoki M,** Lin CL, Rothstein JD, *et al*. Mutations in the glutamate transporter EAAT2 gene do not cause abnormal EAAT2 transcripts in amyotrophic lateral sclerosis. *Ann Neurol* 1998;**43**:645–53.
26. **Brooke MH,** Griggs RC, Mendell JR, *et al*. Clinical trial in Duchenne dystrophy. I. The design of the protocol. *Muscle Nerve* 1981;**4**:186–97.
27. **Nagashima T,** Chuma T, Mano Y, *et al*. Dysferlinopathy associated with rigid spine syndrome. *Neuropathology* 2004;**24**:341–6.
28. **Takahashi T,** Aoki M, Imai T, *et al*. A case of dysferlinopathy presenting choreic movements. *Mov Disord* 2006;**21**:1513–15.

29. **Klinge L,** Dean AF, Kress W, *et al*. Late onset in dysferlinopathy widens the clinical spectrum. *Neuromuscul Disord* 2008;**18**:288–90.
30. **Paradas C,** González-Quereda L, De Luna N, *et al*. A new phenotype of dysferlinopathy with congenital onset. *Neuromuscul Disord* 2009;**19**:21–5.
31. **Nishida Y,** Ishimoto S, Kobayashi T, *et al*. Two sisters with autosomal recessive muscular dystrophy (Miyoshi) with early involvement of limb girdle muscles (in Japanese). *Rinsho Shinkeigaku* 1987;**27**:756–9.
32. **Ueyama H,** Kumamoto T, Horinouchi H, *et al*. Clinical heterogeneity in dysferlinopathy. *Intern Med* 2002;**41**:532–6.
33. **Miyoshi K,** Kawai H, Iwasa M, *et al*. Autosomal recessive distal muscular dystrophy as a new type of progressive muscular dystrophy. *Brain* 1986;**109**: 31–54.
34. **Fisher D,** Walter MC, Kesper K, *et al*. Diagnostic value of muscle MRI in differentiating LGMD2I from other LGMDs. *J Neurol* 2005;**252**:538–47.
35. **Kesper K,** Kornblum C, Reimann J, *et al*. Pattern of skeletal muscle involvement in primary dysferlinopathies: a whole-body 3.0-T magnetic resonance imaging study. *Acta Neurol Scand* 2009;**120**:111–18.
36. **Kuru S,** Yasuma F, Wakayama T, *et al*. A patient with limb girdle muscular dystrophy type 2B (LGMD2B) manifesting cardiomyopathy (in Japanese). *Rinsho Shinkeigaku* 2004;**44**:375–8.
37. **Wenzel K,** Geier C, Qadri F, *et al*. Dysfunction of dysferlin-deficient hearts. *J Mol Med* 2007;**85**:1203–14.
38. **Choi ER,** Park SJ, Choe YH, *et al*. Early detection of cardiac involvement in Miyoshi myopathy: 2D strain echocardiography and late gadolinium enhancement cardiovascular magnetic resonance. *J Cardiovasc Magn Reson* 2010;**12**:31.
39. **Cagliani R,** Fortunato F, Giorda R, *et al*. Molecular analysis of LGMD-2B and MM patients: identification of novel DYSF mutations and possible founder effect in the Italian population. *Neuromuscul Disord* 2003;**13**:788–95.

Journal of Human Genetics (2013), 1–8

www.nature.com/jhg

ORIGINAL ARTICLE

Exome sequencing identifies a novel *TTN* mutation in a family with hereditary myopathy with early respiratory failure

Rumiko Izumi[1,2], Tetsuya Niihori[1], Yoko Aoki[1], Naoki Suzuki[2], Masaaki Kato[2], Hitoshi Warita[2], Toshiaki Takahashi[3], Maki Tateyama[2], Takeshi Nagashima[4], Ryo Funayama[4], Koji Abe[5], Keiko Nakayama[4], Masashi Aoki[2] and Yoichi Matsubara[1]

Myofibrillar myopathy (MFM) is a group of chronic muscular disorders that show the focal dissolution of myofibrils and accumulation of degradation products. The major genetic basis of MFMs is unknown. In 1993, our group reported a Japanese family with dominantly inherited cytoplasmic body myopathy, which is now included in MFM, characterized by late-onset chronic progressive distal muscle weakness and early respiratory failure. In this study, we performed linkage analysis and exome sequencing on these patients and identified a novel c.90263G>T mutation in the *TTN* gene (NM_001256850). During the course of our study, another groups reported three mutations in *TTN* in patients with hereditary myopathy with early respiratory failure (HMERF, MIM #603689), which is characterized by overlapping pathologic findings with MFMs. Our patients were clinically compatible with HMERF. The mutation identified in this study and the three mutations in patients with HMERF were located on the A-band domain of titin, suggesting a strong relationship between mutations in the A-band domain of titin and HMERF. Mutation screening of *TTN* has been rarely carried out because of its huge size, consisting of 363 exons. It is possible that focused analysis of *TTN* may detect more mutations in patients with MFMs, especially in those with early respiratory failure.
Journal of Human Genetics advance online publication, 28 February 2013; doi:10.1038/jhg.2013.9

Keywords: A-band; cytoplasmic body; Fn3 domain; hereditary myopathy with early respiratory failure; HMERF; myofibrillar myopathy; titin; *TTN*

INTRODUCTION

Myofibrillar myopathies (MFMs) were proposed in 1996 as a group of chronic muscular disorders characterized by common morphologic features observed on muscle histology, which showed the focal dissolution of myofibrils followed by the accumulation of products of the degradative process.[1] The clinical phenotype of MFM is characterized by slowly progressive muscle weakness that can involve proximal or distal muscles, with onset in adulthood in most cases. However, other phenotypes are highly variable. Although 20% of patients with MFMs have been revealed to have mutations in *DES*, *CRYAB*, *MYOT*, *LDB* (*ZASP*), *FLNC* or *BAG3*, the major genetic basis of MFMs remains to be elucidated.

Respiratory weakness is one of the symptoms of MFMs. The early or initial presentation of respiratory failure is not a common manifestation of MFMs as a whole, and there are limited reports regarding a fraction of patients with *DES*,[2] *MYOT*[3] or *CRYAB*[4] mutation. In 1993, our group reported a Japanese family with dominantly inherited cytoplasmic body (CB) myopathy,[5] which is now included in MFM. Currently, this family includes 20 patients in five successive generations who show almost homogeneous clinical features characterized by chronic progressive distal muscle weakness and early respiratory failure. However, the underlying genetic etiology in this family was unknown. The aim of this study was to determine the genetic cause in this family. To identify the responsible genetic mutation, we performed linkage analysis and whole-exome sequencing.

MATERIALS AND METHODS

This study was approved by the Ethics Committee of the Tohoku University School of Medicine, and all individuals gave their informed consent before their inclusion in the study.

[1]Department of Medical Genetics, Tohoku University School of Medicine, Sendai, Japan; [2]Department of Neurology, Tohoku University School of Medicine, Sendai, Japan; [3]Department of Neurology and Division of Clinical Research, National Hospital Organization Nishitaga National Hospital, Sendai, Japan; [4]Division of Cell Proliferation, United Centers for Advanced Research and Translational Medicine, Tohoku University Graduate School of Medicine, Sendai, Japan and [5]Department of Neurology, Okayama University Medical School, Okayama, Japan
Correspondence: Dr Y Aoki, Department of Medical Genetics, Tohoku University School of Medicine, 1-1 Seiryo-machi, Aoba-ku, Sendai 980-8574, Japan.
E-mail: aokiy@med.tohoku.ac.jp
or Professor M Aoki, Department of Neurology, Tohoku University School of Medicine, 1-1 Seiryo-machi, Aoba-ku, Sendai 980-8574, Japan.
E-mail: aokim@med.tohoku.ac.jp
Received 23 October 2012; revised 9 January 2013; accepted 10 January 2013

Clinical information on the family

This family includes 20 patients (13 males and 7 females) in five successive generations (Figure 1). The family is of Japanese ancestry, and no consanguineous or international mating was found. Of all patients, seven underwent a muscle biopsy, and two were autopsied. All of the histological findings were compatible with MFM (see clinical data).

The age of onset ranged from 27–45 years. The most common presenting symptom was foot drop. At the initial evaluations, muscle weakness was primarily distributed in the ankle dorsiflexors and finger extensors. The patients were generally built and showed no other extramuscular abnormalities. In addition to this chronic progressive distal muscle weakness, respiratory distress occurred between 0 and 7 years from the initial onset (average 3.8 years) in seven patients (IV-9, V-2, A, B, E, H, and J) with adequate clinical information. Two patients who had not had any respiratory care died of respiratory failure approximately a decade from the initial onset. The other patients have been alive for more than 10 years (maximum 18 years) but require nocturnal non-invasive positive pressure ventilation. They were 37–58 years of age as of 2012 and able to walk independently with or without a simple walking aid. Although the time at which patients recognized dysphagia or dysarthria varied between 1 to more than 10 years from the initial onset, decreased bulbar functions had been noted at the initial evaluation in most cases. Cardiac function was normally maintained in all patients of the family.

Clinical data

The level of serum creatine kinase was normal or mildly elevated. Electromyography of affected muscles showed a chronic myogenic pattern, and the nerve conduction study did not suggest any neuropathic involvement. Muscle imaging showed focal atrophy in the tibialis anterior, tibialis posterior, extensor hallucis and digitorum longus, peroneal and semitendinosus muscle on initial assessment (Figure 2A), and atrophy became clear in cervical muscles, shoulder girdles, intercostals and proximal limb muscles in the following several years. Upon muscle biopsy, the most common finding was numerous cytoplasmic bodies (CBs), which were found on 7.3% of myofibers in the tibialis anterior of individual E (Figure 2B (a–c)) and 50–80% of intercostals in other cases.[5] Other nonspecific findings were increased variability in the size of myofibers, central nuclei and rimmed vacuoles observed on a few fibers. No strong immunoreaction of desmin was seen in the CBs (Figure 2B (d, e)). An electron microscope examination showed that the regular sarcoplasmic pattern was replaced by abnormal fine filamentous structures, which seemed to attach to the Z-band. CBs were also found in almost all skeletal muscles and some smooth muscles in autopsied cases.[5] Cardiac myofibers also contained numerous CBs in one of the autopsied cases (V-2),[5] although the patient did not present any cardiac complication. The sequence analysis of the coding regions and flanking introns of *DES* and *MYOT* showed no pathogenic mutation in individual E. An array comparative genomic hybridization performed with the Agilent SurePrint G3 Human CGH 1M microarray format in individual A did not reveal any aberrations of genomic copy number.

Linkage analysis

DNA was extracted by standard methods. Linkage analysis was performed on nine family members (A–I in Figure 1; four of them were affected, and the others were unaffected) through genotyping using an Illumina Human Omni 2.5 BeadChip (Illumina, San Diego, CA, USA). We chose single-nucleotide polymorphisms (SNPs) that satisfied all of the following criteria: (1) autosomal SNPs whose allele frequencies were available from the HapMap project (http://hapmap.ncbi.nlm.nih.gov/), (2) SNPs that were not monomorphic among members and (3) SNPs that were not in strong linkage disequilibrium with neighboring SNPs (r2 values <0.9). Then, we selected the first five SNPs from each position of integer genetic distance from SNPs that met the above criteria for the initial analysis. The details were as follows; we chose a SNP closest to 0 cM and the neighboring four SNPs. If the genetic distance of a SNP was the same as that of the next SNP, we considered the genomic position to determine their order. We repeated this process at 1 cM, 2 cM and so on.

We performed a multipoint linkage analysis of the data set (17 613 SNPs) using MERLIN[6] 1.1.2 under the autosomal dominant mode with the following parameters: 0.0001 for disease allele frequency, 1.00 for individuals heterozygous and homozygous for the disease allele and 0.00 for individuals

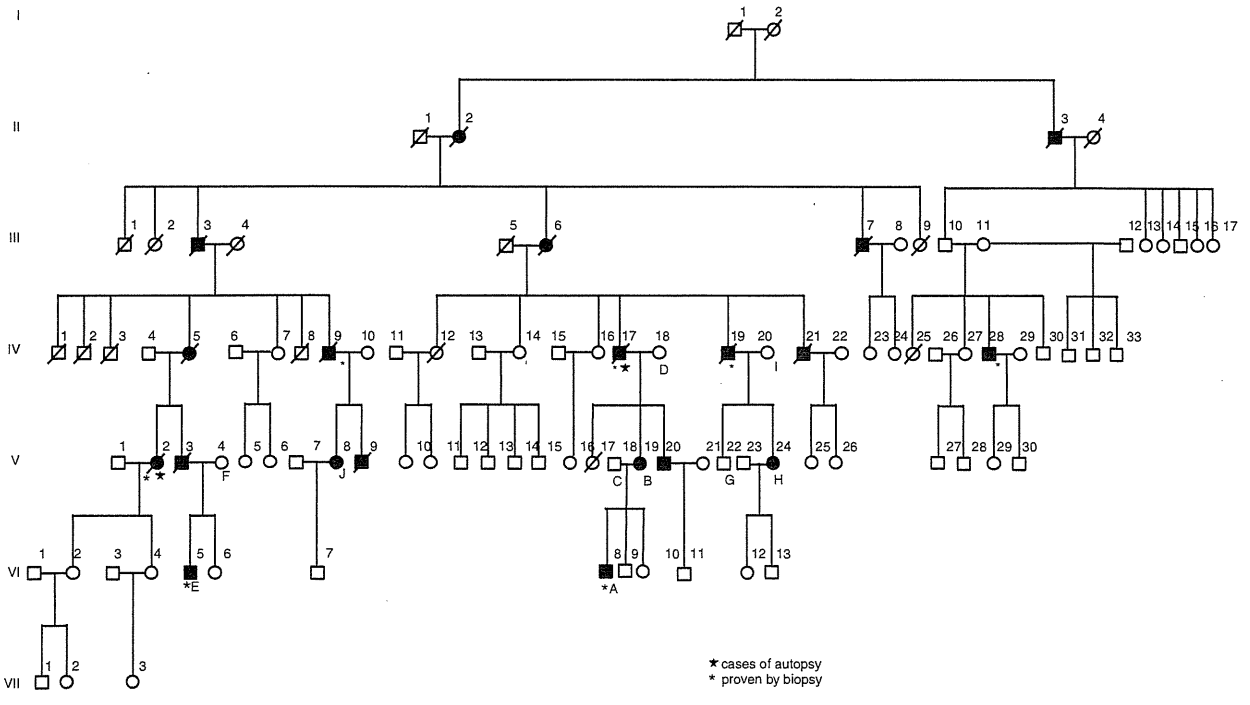

Figure 1 Family pedigree. Filled-in symbols indicate individuals with MFM. Empty symbols indicate unaffected individuals. A star and asterisk indicate autopsy-proven and muscle biopsy-proven cases, respectively. (A–J) indicates individuals whose DNA was used for this study.